

DESIGN OF ULTRA-WIDEBAND (2-18 GHz) BUTLER MATRIX

A Thesis

by

INDERDEEP SINGH

Submitted to the Office of Graduate and Professional Studies of
Texas A&M University
in partial fulfillment of the requirements for the degree of

MASTER OF SCIENCE

Chair of Committee,	Gregory H. Huff
Co-Chair of Committee,	Robert D. Nevels
Committee Members,	Jean-Francois Chamberland Darren Hartl
Head of Department,	Miroslav M. Begovic

December 2019

Major Subject: Electrical Engineering

Copyright 2019 Inderdeep Singh

ABSTRACT

This thesis presents the design of an ultra-wide band hybrid coupler, crossover and phase shifters for the design of four-input, four-output (4x4) stripline Butler matrix in order to feed an antenna array in 2-18 GHz frequency range. The goal of this thesis is to develop an antenna-array feeding passive microwave network based on Butler matrix with a ultra-wide bandwidth which works as ground work for realization of eight input, eight output Butler matrix. Further the 4x4 and 8x8 Butler matrix can be used in a row-card configuration to realize 16x16 and 64x64 Butler matrix. In order to meet the ultra-wide band requirements, wide band passive microwave components such as hybrid coupler, crossovers and phase-shifters are designed, which operate from 2 to 18 GHz. The Butler matrix can be used as a beam-forming network produces orthogonal beams which can be steered in different directions.

ACKNOWLEDGEMENTS

I would like to thank my committee chair, Dr. Gregory Huff, my co-chair Dr. Robert Nevels and my committee members, Dr. Jean-Francois Chamberland and Dr. Darren Hartl for their guidance and support throughout the course of this research.

Thanks also go to my friends and colleagues and the department faculty and staff for making my time at Texas A&M University a great experience.

Finally, thanks to family for their constant encouragement.

CONTRIBUTORS AND FUNDING SOURCES

This work was supervised by a thesis committee consisting of Professors Gregory H. Huff (advisor), Robert D. Nevels and Jean-Francois Chamberland of the Department of Electrical and Computer Engineering and Professor Darren Hartl of the Department of Aerospace Engineering.

All work for the thesis was completed independently by the student.

There are no outside funding contributions to acknowledge related to the research and compilation of this document.

TABLE OF CONTENTS

	Page
ABSTRACT	ii
ACKNOWLEDGEMENTS	iii
CONTRIBUTORS AND FUNDING SOURCES.....	iv
TABLE OF CONTENTS	v
LIST OF FIGURES.....	vii
1. INTRODUCTION.....	1
1.1. Butler Matrix	2
1.2. 90° Hybrid Coupler	5
1.3. Crossover.....	6
1.4. Phase Shifters	8
2. HYBRID COUPLER	9
2.1. Coupling Structures.....	9
2.2. Even and Odd Mode Impedances.....	11
2.3. Braodband Couplers.....	14
2.4. Coupler Design.....	22
3. CROSSOVER DESIGN.....	31
4. PHASE SHIFTER DESIGN	34
5. 4X4 BUTLER MATRIX DESIGN AND RESULTS	44
6. FUTURE WORK	50
6.1. TRL Calibration Kit	50
6.2. 8X8 Butler Matrix	53
6.3. 16X16 Butler Matrix	54
6.4. 64X64 Butler Matrix	58
7. CONCLUSIONS	59

REFERENCES..... 60

LIST OF FIGURES

	Page
Figure 1-1 : 2x2 Butler Matrix Schematic	3
Figure 1-2 : 4x4 Butler matrix schematic.....	4
Figure 1-3 : 8x8 Butler matrix schematic.....	4
Figure 1-4 : Hybrid Coupler	5
Figure 1-5 : Crossover as Tandem Connection of Hybrid Couplers.....	6
Figure 2-1 : Coupled transmission lines (a) edge coupled microstrip, (b) edge coupled striplines, (c) broadside coupled striplines, (d) offset coupled striplines.....	10
Figure 2-2 : Representation of capacitances on coupled lines	12
Figure 2-3 : Even mode excitation of coupled lines.....	12
Figure 2-4 : Odd mode excitation in coupled lined.....	13
Figure 2-5 : Slot Coupled Microstrip Coupler	16
Figure 2-6 : Magnitude response of single section slot coupled microstrip coupler...	16
Figure 2-7 : 3-Section slot coupled microstrip coupler.....	17
Figure 2-8 : Magnitude and phase response of 3-section slot coupled microstrip coupler (a) Magnitude Response (b) Phase Response.....	18
Figure 2-9 : 5-Section slot coupled microstrip coupler.....	19
Figure 2-10 : Magnitude Response of 5-section slot coupled microstrip coupler.....	19
Figure 2-11 : 3 dB coupler as a tandem connection of two 8.34 dB couplers	21
Figure 2-12 : 7-section 8.34 dB stripline coupler (a) Top view (b) Trimetric view ...	26
Figure 2-13 : Geometry of stripline structures	26
Figure 2-14 : Magnitude and phase response of 7-section 8.34 dB coupler (a) Magnitude response (b) Phase response	27

Figure 2-15 : 3 dB coupler as a tandem connection of two 8.34 dB couplers (a) Top view (b) Trimetric view	28
Figure 2-16 : Magnitude and phase response of 3 dB coupler	29
Figure 3-1 : Crossover design as a tandem connection of two 3 dB couplers (a) Top View (b) Trimetric View	32
Figure 3-2 : Crossover magnitude response	33
Figure 4-1 : Schiffman phase shifter	34
Figure 4-2 : Phase response of single section 90° Schiffman phase shifters	36
Figure 4-3 : 5-section Schiffman phase shifter with a straight reference line.....	38
Figure 4-4 : Schiffman phase shifter with reference line showing the de-embed.....	38
Figure 4-5 : Phase response of 5-section 45 degrees Schiffman phase shifter with respect to a straight line	39
Figure 4-6 : Phase shifter with extra lengths to compensate for crossover phase response	40
Figure 4-7 : Phase response of 5-section 45 degrees Schiffman phase shifter with respect to crossover.....	41
Figure 4-8 : Phase response of 6-section 45 degrees Schiffman phase shifter with respect to crossover.....	41
Figure 4-9 : Phase response of 6-section 67.5 degrees Schiffman phase shifter with respect to crossover.....	42
Figure 4-10 : Phase response of 6-section degrees Schiffman phase shifter with respect to crossover.....	43
Figure 5-1 : Layout of 4x4 ultra-wideband Butler matrix (Top View).....	45
Figure 5-2 : Layout of ultra-wideband Butler matrix (Trimetric view)	46
Figure 5-3 : Magnitude Response of Butler matrix with respect to Port 1	47
Figure 5-4 : Magnitude response of Butler matrix with respect to Port 2.....	47
Figure 5-5 : Butler Matrix progressive phase shifts of 45° with respect to Port 1	48

Figure 5-6 : Butler Matrix progressive phase shifts of 135° with respect to Port 2....	49
Figure 6-1 : Through standard.....	50
Figure 6-2 : Reflect standard.....	51
Figure 6-3 : Line standards.....	51
Figure 6-4 : Two-port response of hybrid coupler without calibration kit.....	52
Figure 6-5 : Two-port response of hybrid coupler with calibration kit.....	53
Figure 6-6 : Schematic view of row card configuration of 16x16 Butler matrix from 4x4 Butler matrix.....	55
Figure 6-7 : Designed 4x4 Butler matrix stacked in row-card configuration to form 16x16 Butler matrix.....	55
Figure 6-8 : Circuit schematic of 16x16 Butler matrix from 4x4 Butler matrices.....	56
Figure 6-9 : Ideal magnitude response of 16x16 Butler matrix designed as row card configuration of 4x4 Butler matrix.....	57
Figure 6-10 : Ideal phase response of 16x16 Butler matrix designed as row card configuration of 4x4 Butler matrix.....	57
Figure 6-11 : Schematic view of row card configuration of 64x64 Butler matrix from 8x8 Butler matrix.....	58

1. INTRODUCTION

Beam-forming or spatial filtering techniques have an extensive range of applications including but not limited to defense [1, 2], automotive communications [3] and cellular communications [4]. The upcoming 5G technology for cellular communication has strong dependence on beam-forming to form a direct link between the receiver and sender to counter the attenuation of millimeter waves [5]. A beam-forming network generates the required amplitude and phase excitations, to steer the radiated beam to a specific spatial direction without changing the physical locations of the antenna elements. Examples include, the digital beam-forming networks [6], the circuit based beam-forming networks such as Butler Matrix [7] and Blass Matrix [8] and the Microwave lens beam-forming networks such as Rotman lens [9] and Luneberg lens [10] .

While digital beam-forming networks provide better performance with very low phase errors and more flexible amplitude tapering, they are not suitable for high frequencies and requires large hardware and enormous power as the aperture size or the number of antenna elements increase. Butler matrix network is easy to construct and implement on printed circuit boards. By varying the input current amplitude and input phase to the Butler matrix the beam can be scanned to the required direction. Sheleg discusses the design and implementation of Butler matrix based scanning using circular array [11]. Tayeb *et al.* described a 4x4 Butler matrix design for linear microstrip antenna array operating at 1.9 GHz [12]. Mourad *et al.* have designed 4x4 Butler matrix

using coplanar waveguides at 5.8 GHz [13]. In this work ultra-wideband (2-18 GHz) stripline Butler matrix design is proposed. Individual building blocks, hybrid coupler, crossover, phase shifter are first designed for 2-18 GHz. Further they are put together to form 4x4 Butler matrix.

1.1. Butler Matrix

A butler matrix is a passive microwave beamforming network used to feed a phased antenna array. It was first proposed by Butler and Lowe in 1961 [14]. To steer the beam using a phased antenna array, current phase needs to be varied. Each antenna element in the phased array can be fed with progressive phase shifts to steer the beam in a specific direction. Butler matrix facilitates this operation by feeding current to the antenna elements in a progressive phase shift manner.

A Butler matrix is an N-input N-output passive microwave network, where N is generally some power of 2. Power is applied at the N-input ports and the progressive phase shifts are obtained at the N-output ports to which N antenna elements are connected. The N-input ports are also called the beam ports and the N-output ports are called the antenna ports. The beam direction can be controlled by which input or beam port is excited. The input at any one beam port results in current of equal amplitude and linearly varying phase at the antenna ports. This kind of operation is generally called switched beam, where the input is switched to one of the beam ports. Multiple beam ports can also be simultaneously fed. For example, if two ports are fed simultaneously, the antenna array radiates dual beams simultaneously, superimposed on one another.

The phase difference between the antenna ports varies depending on which beam port is excited. In general for an N-input port Butler matrix if K th ($K = \pm 1, \pm 2, \pm 3, \dots, \pm N/2$) port is excited the phase difference between output ports is $\pm (2K-1)/N$. For the simple case of 2x2 Butler matrix the phase difference between output ports is $\pm 90^\circ$. Therefore a 2x2 Butler matrix is simply a 90° hybrid coupler. **Figure 1-1** shows a block diagram of such a Butler matrix. In general N-port Butler matrix is a passive network formed by a combination of 90° hybrid couplers, crossovers and phase shifters.

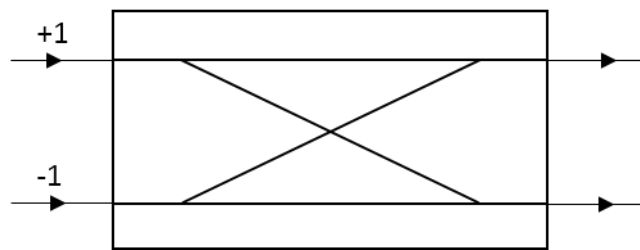


Figure 1-1 : 2x2 Butler Matrix Schematic

Figure 1-2 shows the block diagram of a 4x4 Butler matrix. It requires a crossover, four hybrid couplers and two 45° phase shifters. Extending the idea to 8x8 Butler, it requires 12 hybrid couplers, ten crossovers, two 67.5° phase shifters, two 22.5° phase shifters and four 45° phase shifters. **Figure 1-3** shows the block diagram for the same.

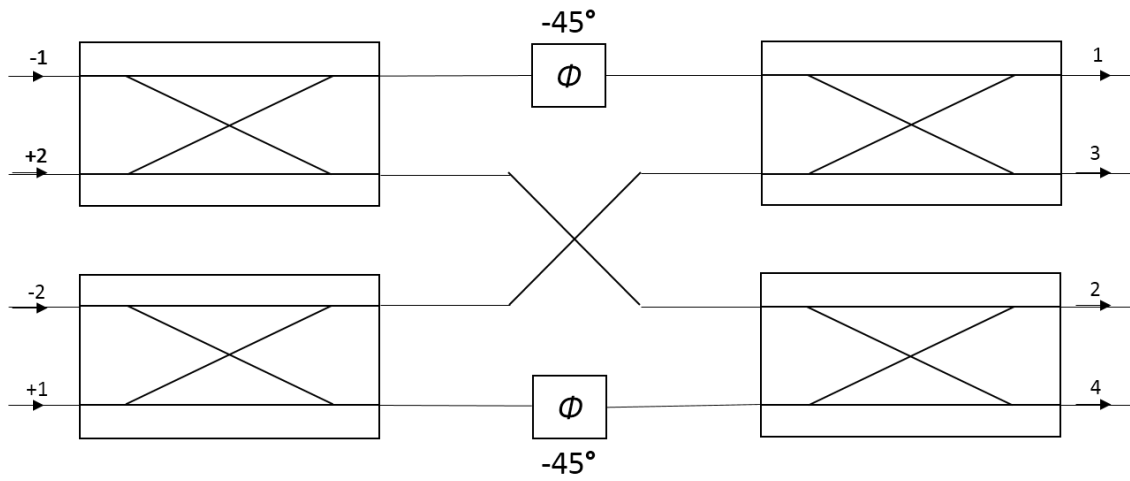


Figure 1-2 : 4x4 Butler matrix schematic

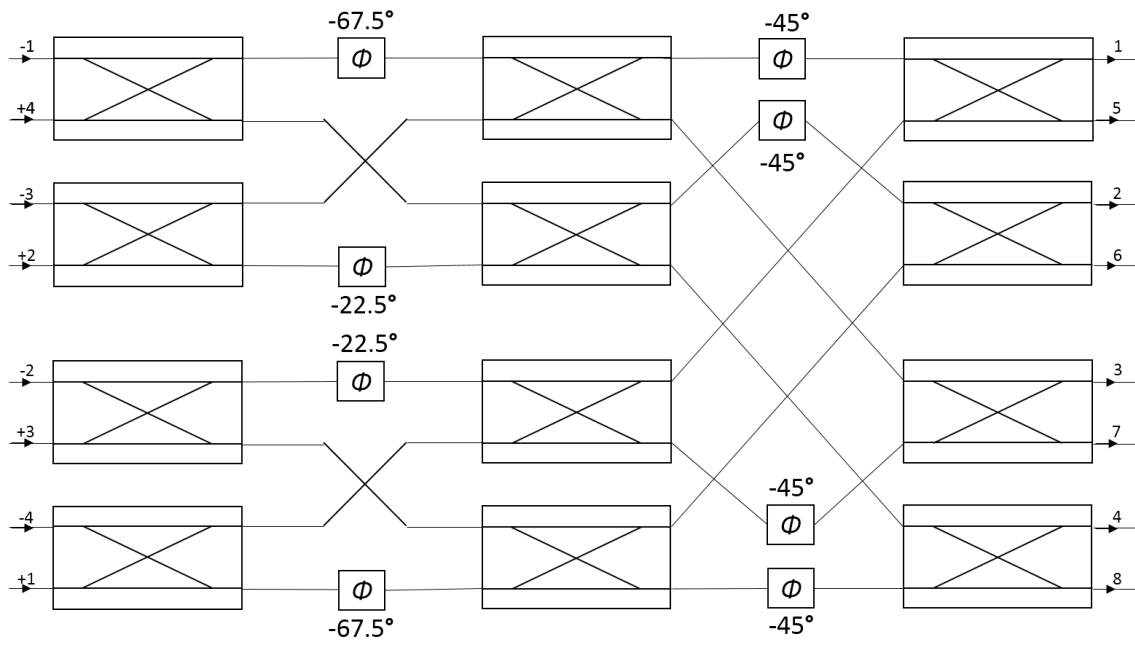


Figure 1-3 : 8x8 Butler matrix schematic

1.2. 90° Hybrid Coupler

A hybrid coupler is a four port passive microwave device, which splits the input signal into two equi-power signals at outputs and the fourth port is isolated. It is a special case of directional coupler such that the coupling is 3 dB or half power split at the outputs. For a 90° hybrid coupler the outputs differ in phase by 90°. **Figure 1-4** shows the block diagram of a hybrid coupler. Port 1 is the “input” port; coupled power goes to port 3 or the “coupling” port. Rest of the power goes directly to port 2 or the “through” port while port 4 is the “isolation” port. Ideally no power shows up at isolation port. So, for a 90° hybrid coupler power at port 1 splits into equally to port 2 and 3, with a phase difference of 90° between port 2 and 3.

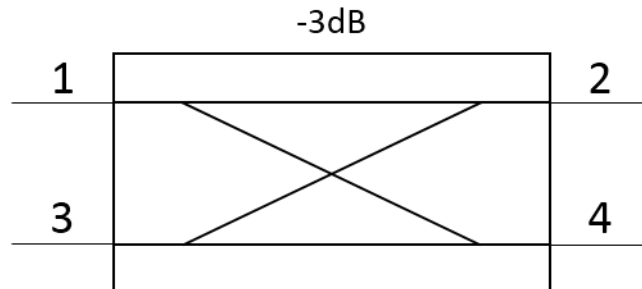


Figure 1-4 : Hybrid Coupler

S-matrix of a general coupler is written as:

$$\begin{bmatrix} 0 & -j \cos \alpha & \sin \alpha & 0 \\ -j \cos \alpha & 0 & 0 & \sin \alpha \\ \sin \alpha & 0 & 0 & -j \cos \alpha \\ 0 & \sin \alpha & -j \cos \alpha & 0 \end{bmatrix} \quad (1-1)$$

where $\sin \alpha = k$ is the voltage coupling coefficient. For the hybrid coupler, since coupled power is $\frac{1}{2}$ therefore the voltage coupling coefficient, k becomes $\sqrt{\frac{1}{2}}$ or $\alpha = \pi/4$.

Based on the application, the frequency of operation, 90° hybrid coupler can be realized as coupled line coupler, branchline coupler, Lange coupler or interdigitated coupler etc. in transmission line structures such as microstrip, stripline, waveguide etc. Section 2 covers the design choices available for this particular application where 3 dB coupling is required over 2-18 GHz and the finalized stripline design with its simulated results in HFSS.

1.3. Crossover

Crossover can be realized by connecting two 90° hybrid couplers in tandem, such as shown in **Figure 1-5** where port 2 of first coupler is connected to port 4' of second coupler and port 3 of first coupler to port 1' of second coupler.

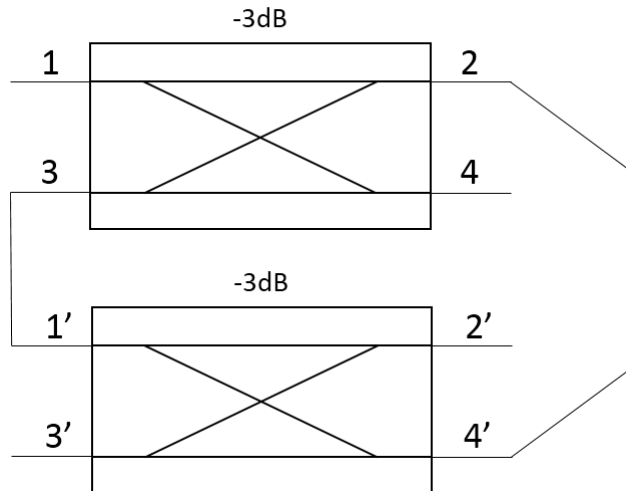


Figure 1-5 : Crossover as Tandem Connection of Hybrid Couplers

When input port of the first coupler is excited by a unity wave voltage, the voltage waves amplitude and phase at the other ports can be obtained using the S-matrix of the 90° hybrid. Using voltage coupling coefficient of $k = \sqrt{1/2}$,

$$\begin{bmatrix} V_1^- \\ V_2^- \\ V_3^- \\ V_4^- \end{bmatrix} = \begin{bmatrix} 0 & -j\sqrt{1/2} & \sqrt{1/2} & 0 \\ -j\sqrt{1/2} & 0 & 0 & \sqrt{1/2} \\ \sqrt{1/2} & 0 & 0 & -j\sqrt{1/2} \\ 0 & \sqrt{1/2} & -j\sqrt{1/2} & 0 \end{bmatrix} \begin{bmatrix} 1 \\ 0 \\ 0 \\ 0 \end{bmatrix} \quad (1-2)$$

which gives,

$$V_1^- = 0 \quad (1-3)$$

$$V_2^- = -j\sqrt{1/2} \quad (1-4)$$

$$V_3^- = \sqrt{1/2} \quad (1-5)$$

$$V_4^- = 0 \quad (1-6)$$

Now, V_2^- and V_3^- are the incident voltage waves at port 1 and port 4 of the second coupler, therefore the reflected voltages of coupler 2 can be obtained as:

$$\begin{bmatrix} V_1'^- \\ V_2'^- \\ V_3'^- \\ V_4'^- \end{bmatrix} = \begin{bmatrix} 0 & -j\sqrt{1/2} & \sqrt{1/2} & 0 \\ -j\sqrt{1/2} & 0 & 0 & \sqrt{1/2} \\ \sqrt{1/2} & 0 & 0 & -j\sqrt{1/2} \\ 0 & \sqrt{1/2} & -j\sqrt{1/2} & 0 \end{bmatrix} \begin{bmatrix} 0 \\ -j\sqrt{1/2} \\ \sqrt{1/2} \\ 0 \end{bmatrix} \quad (1-7)$$

which leads to,

$$V_1'^- = 0 \quad (1-8)$$

$$V_2'^- = -j \quad (1-9)$$

$$V_3'^- = 0 \quad (1-10)$$

$$V_4'^- = 0 \quad (1-11)$$

According to the analysis above, when two hybrids are connected in tandem all of the input power comes out through port 2 of the second coupler.

Hence design of crossover for the realization of Butler matrix is straightforward once design topology of 90° hybrid coupler is fixed.

1.4. Phase Shifters

Phase shifters are critical components in numerous RF systems including linear power amplifiers (Doherty amplifier) and phased array systems as in this application. For Butler Matrix the phase shift required as shown in **Figure 1-2** and **Figure 1-3** are with respect to the crossovers and any extra line lengths that can be attributed to the layout of Butler Matrix. For broadband designs, challenge lies in designing phase shifters that can provide a flat phase shift throughout the bandwidth of interest, ie. 2-18 GHz.

Ideally, the power at the output of phase shifter should be equal to the input power, which implies an insertion loss of 0 dB. But due to the finite non-ideal transmission line length, there are dielectric and conductor losses which degrade the insertion loss. These losses are more significant at higher frequencies.

2. HYBRID COUPLER

As described on last section, hybrid coupler is one of the key building blocks for the design of Butler matrix. For this design, the frequency of operation is 2-18 Ghz, hence the an ultra-wideband 90° hybrid coupler is required with 3dB coupling and 90° phase difference between the through and coupled ports over the entire frequency range. The challenge of the design inherently lies in the ultra-wideband operation. Such wide bandwidth of operation is practically not possible with a single section coupler.

2.1. Coupling Structures

When two or more transmission lines are present in close proximity to each other, due to the interaction of electric and magnetic fields, power from one line is coupled to another. Specifically, in a two transmission line system, if the primary transmission line is excited, power couples to the secondary transmission line. The coupled power is a function of the dimensions of the transmission lines, dielectric media, mode of propagation and frequency of operation. Such coupling structures could either be edge coupled, broadside coupled or offset coupled as shown in **Figure 2-1**. Since microstrip lines lie in the same plane they can only be design as edge coupled.

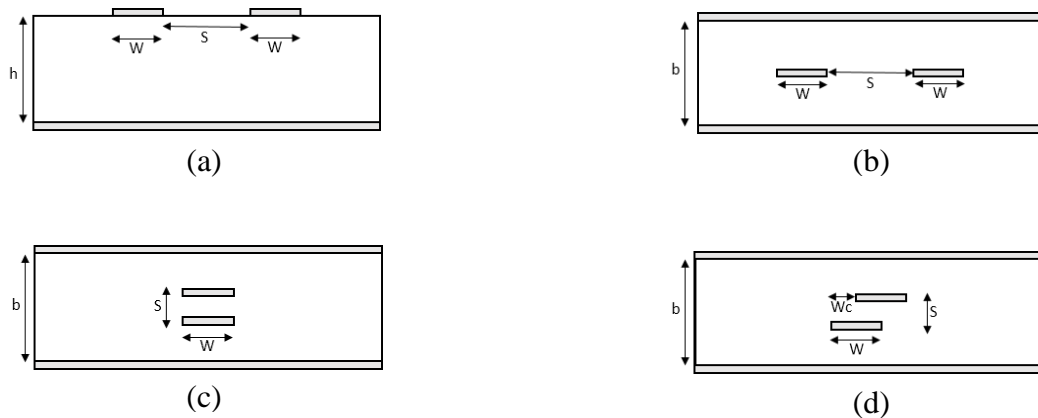


Figure 2-1 : Coupled transmission lines (a) edge coupled microstrip, (b) edge coupled striplines, (c) broadside coupled striplines, (d) offset coupled striplines

Closer the two lines, stronger is the interaction between the electromagnetic fields of the two lines, hence higher coupling can be achieved. Similarly, large interfacing area of the lines results in higher coupling. Which results in broadside coupled lines being coupled tighter as compared to edge coupled lines. For edge-coupled transmission lines, practical spacing limitations between the two lines limit the maximum coupling achievable using a single quarter-wave ($\lambda/4$) section to around 8dB. Whereas, a broadside coupled single section of $\lambda/4$ length can result in 3dB or even tighter coupling.

The separation and the dimensions of the two transmission lines can be also be variable throughout the length of the coupled section. If the dimensions of the lines are equal, and they have constant separation between them, such lines are called symmetric and uniformly coupled lines. A structure with varying separation is called non-uniformly

coupled lines and structure with varying widths of lines is called asymmetric coupled lines.

The coupling between the two coupled transmission lines is described in terms of even and odd modes of excitation. In even-mode excitation the two transmission lines are at equal potentials and in odd-mode the lines are at equal but opposite polarity potential. The coupling is defined in terms of characteristic impedances of these two modes. When both lines are excited in phase with equal amplitude (even-mode), the impedance from one line to the ground is the even-mode characteristic impedance (Z_{0e}). Similarly, when the lines are excited in opposite phase but equal amplitude (odd-mode), the impedance from one line to ground is the odd-mode characteristic impedance (Z_{0o}). Voltage coupling coefficients of the coupled line structures are expressed in terms of these even and odd-mode characteristic impedances, length of the coupled structures and the effective dielectric constant. For homogenous transmission lines of $\lambda/4$ length, the voltage coupling coefficient, k is

$$k = \frac{Z_{0e} - Z_{0o}}{Z_{0e} + Z_{0o}} \quad (2-1)$$

2.2. Even and Odd Mode Impedances

Let's consider two coupled transmission lines with common ground, three types of capacitances are associated with such a system as shown in **Figure 2-2**. V_1, Q_1 and V_2, Q_2 are the voltages and charges on the two coupled lines respectively. The relationship between the capacitances, voltages and charges can be written as,

$$Q_1 = C_{11}V_1 + C_{12}(V_1 - V_2) \quad (2-2)$$

$$Q_2 = C_{22}V_2 + C_{12}(V_2 - V_1) \quad (2-3)$$

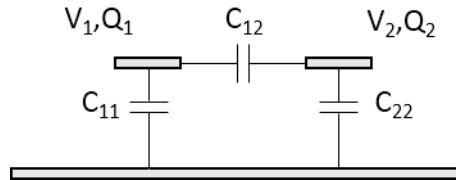


Figure 2-2 : Representation of capacitances on coupled lines

For even mode excitation equal amplitude and in phase voltages ($V_1 = V_2 = V_e$) are applied to the two lines. Due to the symmetrical structure, if equal voltages are applied the charges would also be equal, $Q_1 = Q_2 = Q_e$. This will result in the two capacitances C_{11} and C_{22} to be equal. C_{12} can be divided into two series capacitances $2C_{12}$ and a virtual open or magnetic ground is created at the plane of symmetry as shown in **Figure 2-3**. Thus the two series capacitance can be “disconnected”. For even mode, the capacitance of one line in even mode, C_e can be written as,

$$C_e = C_{11} = C_{22} = \frac{Q_e}{V_e} \quad (2-4)$$

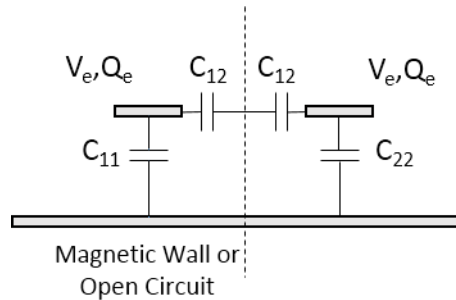


Figure 2-3 : Even mode excitation of coupled lines

For odd mode excitation equal amplitude and opposite phase voltages ($V_1 = -V_2 = V_o$) are applied to the two lines. Again due to the symmetry, the charges would also be equal and opposite in polarities, $Q_1 = -Q_2 = Q_o$. C_{12} can be divided into two series

capacitances $2C_{12}$ and a virtual ground or electric ground is created the plane of symmetry as shown in **Figure 2-4**. Thus,

$$Q_o = (C_{11} + 2C_{12})V_o \quad (2-5)$$

or

$$C_o = (C_{11} + 2C_{12}) = \frac{Q_o}{V_o} \quad (2-6)$$

where C_o is the capacitance of one line for odd mode excitation.

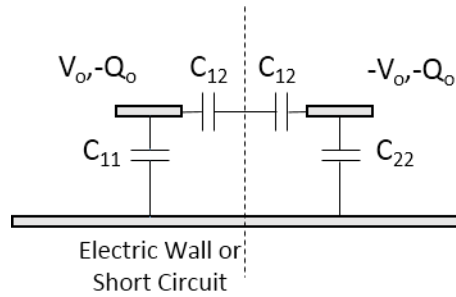


Figure 2-4 : Odd mode excitation in coupled lined

The magnetic wall and electric wall plane of symmetry for even and odd modes respectively make the analysis of calculating capacitances C_e and C_o easier by just considering half the structure.

Characteristic impedance of transmission line is related to capacitance per unit length,

$$Z_0 = \frac{1}{v_p C} \quad (2-7)$$

Where v_p is the phase velocity,

$$v_p = \frac{c}{\sqrt{\epsilon_r}} \quad (2-8)$$

Therefore even and odd mode characteristic impedances are,

$$Z_{0e} = \frac{1}{v_{pe} C_e} \quad (2-9)$$

and

$$\mathbf{Z}_{0o} = \frac{1}{v_{po} C_o} \quad (2-10)$$

For homogeneous transmission lines such as striplines, the phase velocities of even and odd modes are equal,

$$v_{pe} = v_{po} = \frac{c}{\sqrt{\epsilon_r}} \quad (2-11)$$

For inhomogeneous transmission lines, for instance microstrip transmission lines, the even and odd mode phase velocities are generally unequal,

$$v_{pe} = \frac{c}{\sqrt{\epsilon_{re}}} \quad (2-12)$$

and

$$v_{po} = \frac{c}{\sqrt{\epsilon_{ro}}} \quad (2-13)$$

Where ϵ_{re} and ϵ_{ro} are effective even and odd mode dielectric constants.

2.3. Braodband Couplers

Multiple sections of quarter wave coupled lines can be cascaded, in order to achieve near constant coupling over a wide bandwidth. It involves appropriate selection of even and odd-mode impedances of each section. The relation between even- and odd-mode impedance of each section is related by,

$$\mathbf{Z}_0^2 = \mathbf{Z}_{0e} \mathbf{Z}_{0o} \quad (2-14)$$

where \mathbf{Z}_0 is the impedance of terminating ports of the coupler.

A symmetrical broadband coupler has odd number of sections. In such a coupler the i th section is identical to the $N+1-i$ th section and thus is symmetric around the middle section. An asymmetric coupler lacks such symmetry and can employ even or odd number of sections. In the case of symmetrical couplers the through and coupled ports are 90° apart in phase, a property required for the design of Butler matrix.

In [15] Cristal and Young tabulated even and odd mode impedances, of each section of multi-section coupler for number of sections, coupling coefficients and fractional bandwidth for symmetrical TEM mode coupled lines. One way to realize the required 90° hybrid coupler could be in microstrip multi-section edge coupled lines. But the amount of coupling required for the middle sections is too high to be physically realizable. For a practical realization of edge coupled microstrip lines, it is very hard to achieve less than 8 dB of coupling since it requires too small spacing between the lines. Moreover, transmission mode in microstrip lines is not purely TEM due to inhomogeneous dielectric (air and the dielectric medium). The phase velocities of odd and even mode are not equal, which leads to phase errors between the through and coupled ports. [16] Employed wiggly lines in order to get equal phase velocities for even- and odd- mode. Due to restriction in achievable coupling requirement of the tightly coupled middle section, edge coupled micro-strip lines are not suitable for this work.

For tighter coupling [17] proposed Lange or interdigitated couplers by increasing the mutual capacitance between the lines. Interdigitated couplers are sensitive to small gaps between the conductors. Also, it requires bond wires which can cause manufacturing issues.

More recently [18] used slot coupled microstrip lines to achieve tighter coupling over 3.1 to 10.6 GHz. It was followed by [19] where three sections were used to achieve even higher bandwidth from 2.3 to 12.3 GHz. Using this design paradigm, a broadband coupler was designed for our application for 2-18 GHz operation. **Figure 2-5**

shows the single section design and **Figure 2-6** shows its magnitude response.

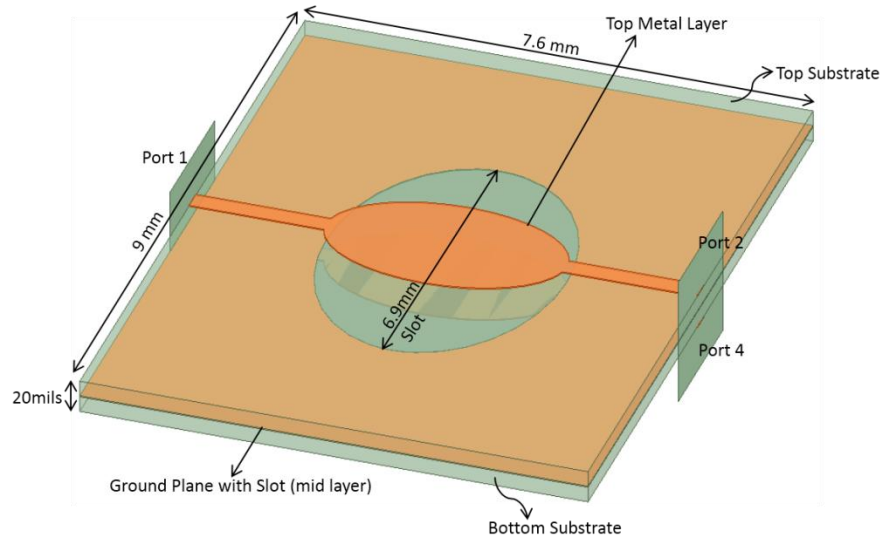


Figure 2-5 : Slot Coupled Microstrip Coupler

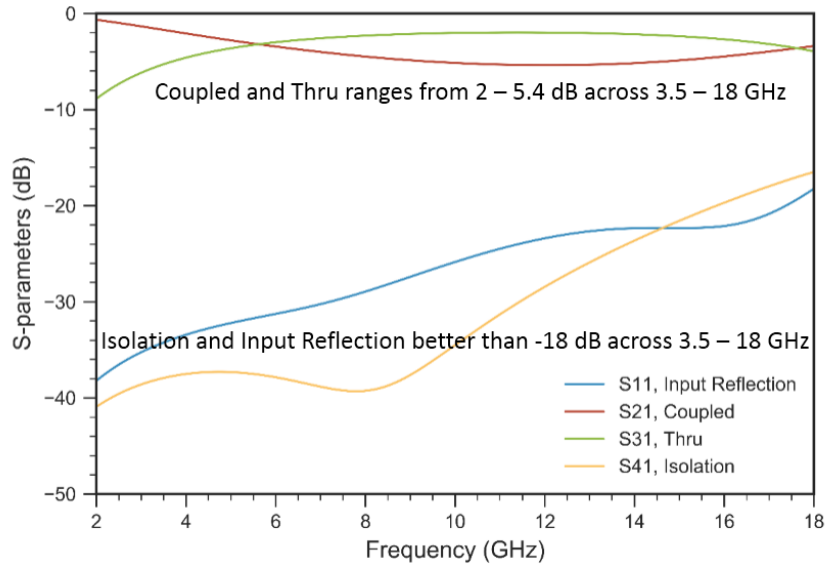


Figure 2-6 : Magnitude response of single section slot coupled microstrip coupler

Figure 2-7 shows the designed 3-section coupler followed by its magnitude and phase response in **Figure 2-8**. Although the phase response of these couplers are decent with error within 5 degrees, but the coupling achieved is not sufficient. It ranges from 1.8 to 5.8 dB, which ideally should have been 3 dB.

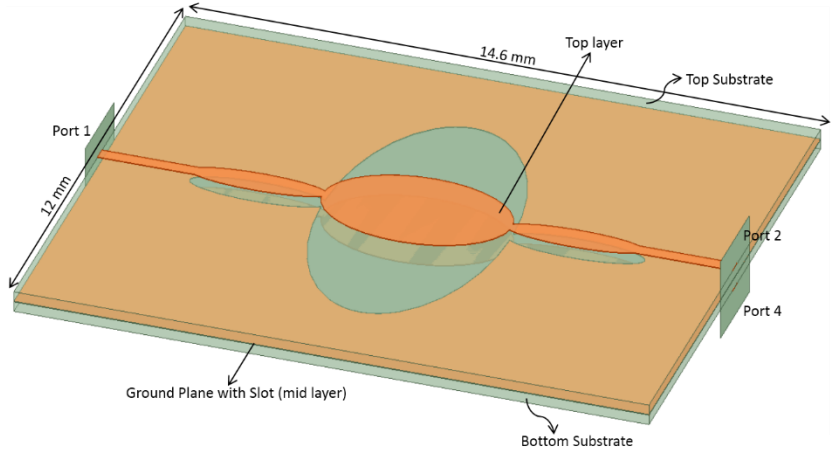
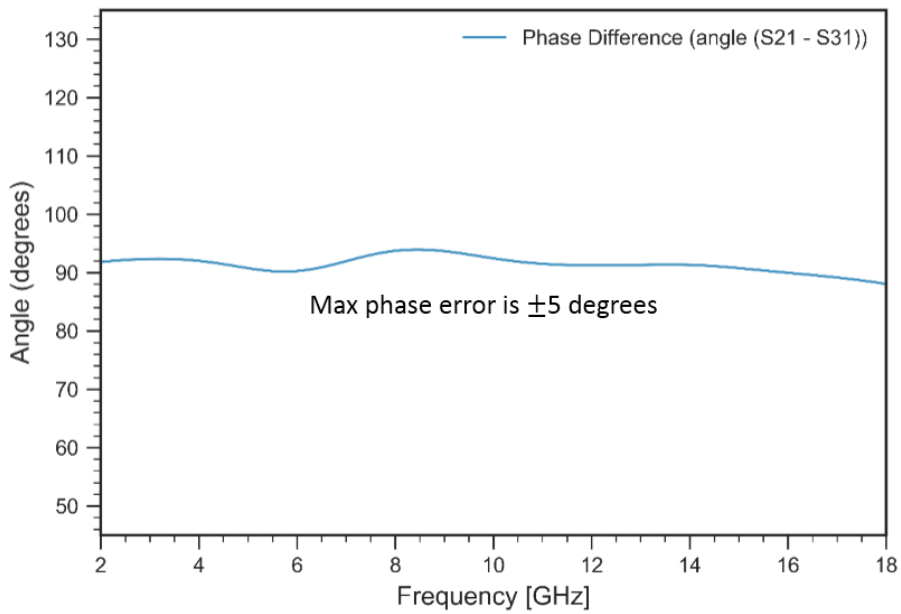


Figure 2-7 : 3-Section slot coupled microstrip coupler



(a)



(b)

Figure 2-8 : Magnitude and phase response of 3-section slot coupled microstrip coupler (a) Magnitude Response (b) Phase Response

This design was further extended to 5 sections as shown in **Figure 2-9** in order to achieve a tighter coupling, but the desired coupling could not be achieved at higher frequencies as shown in **Figure 2-10**.

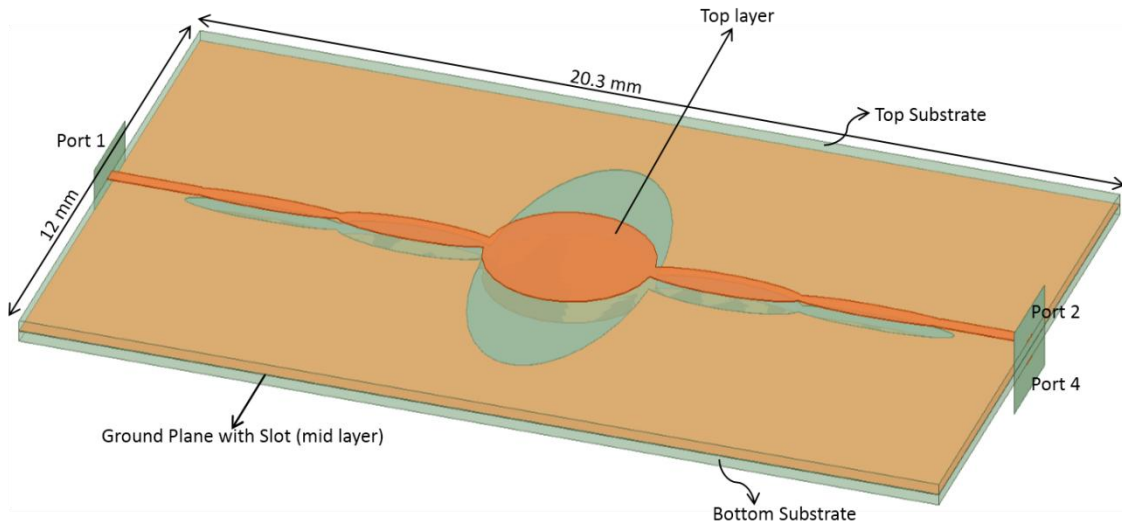


Figure 2-9 : 5-Section slot coupled microstrip coupler

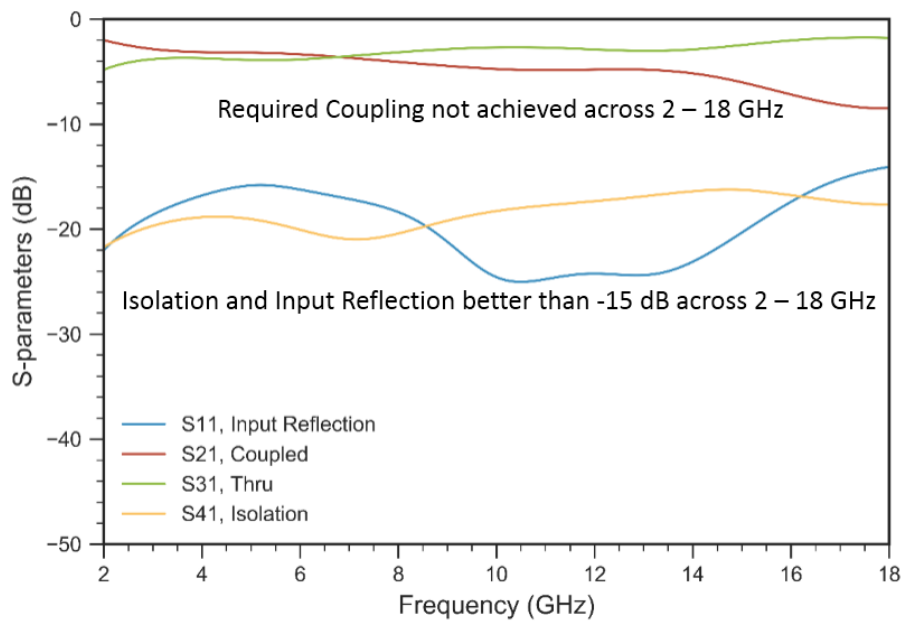


Figure 2-10 : Magnitude Response of 5-section slot coupled microstrip coupler

Another way to design a tight coupler is to connect two loose couplers in tandem. By connecting two 8.34 dB couplers in tandem a tight coupling of 3 dB is achieved. This can be shown using a similar analysis as done in Section 1.3. The S-matrix of first hybrid coupler is,

$$\begin{bmatrix} \mathbf{0} & -j \cos \alpha_1 & \sin \alpha_1 & \mathbf{0} \\ -j \cos \alpha_1 & \mathbf{0} & \mathbf{0} & \sin \alpha_1 \\ \sin \alpha_1 & \mathbf{0} & \mathbf{0} & -j \cos \alpha_1 \\ \mathbf{0} & \sin \alpha_1 & -j \cos \alpha_1 & \mathbf{0} \end{bmatrix} \quad (2-15)$$

And similarly S-matrix of second hybrid coupler is given by

$$\begin{bmatrix} \mathbf{0} & -j \cos \alpha_2 & \sin \alpha_2 & \mathbf{0} \\ -j \cos \alpha_2 & \mathbf{0} & \mathbf{0} & \sin \alpha_2 \\ \sin \alpha_2 & \mathbf{0} & \mathbf{0} & -j \cos \alpha_2 \\ \mathbf{0} & \sin \alpha_2 & -j \cos \alpha_2 & \mathbf{0} \end{bmatrix} \quad (2-16)$$

Where $\sin \alpha_1$ and $\sin \alpha_2$ are the voltage coupling coefficients of the two hybrid couplers. When input port of the first coupler is excited by a wave voltage of amplitude one, the reflected voltages obtained using the S-parameter are,

$$\begin{bmatrix} V_1^- \\ V_2^- \\ V_3^- \\ V_4^- \end{bmatrix} = \begin{bmatrix} \mathbf{0} & -j \cos \alpha_1 & \sin \alpha_1 & \mathbf{0} \\ -j \cos \alpha_1 & \mathbf{0} & \mathbf{0} & \sin \alpha_1 \\ \sin \alpha_1 & \mathbf{0} & \mathbf{0} & -j \cos \alpha_1 \\ \mathbf{0} & \sin \alpha_1 & -j \cos \alpha_1 & \mathbf{0} \end{bmatrix} \begin{bmatrix} \mathbf{1} \\ \mathbf{0} \\ \mathbf{0} \\ \mathbf{0} \end{bmatrix} \quad (2-17)$$

$$V_1^- = \mathbf{0} \quad (2-18)$$

$$V_2^- = -j \cos \alpha_1 \quad (2-19)$$

$$V_3^- = \sin \alpha_1 \quad (2-20)$$

$$V_4^- = \mathbf{0} \quad (2-21)$$

For the second hybrid V_2^- and V_3^- are the incident voltage waves at port 1 and port 4, and using S-parameters of the second hybrid coupler,

$$\begin{bmatrix} V_1' \\ V_2' \\ V_3' \\ V_4' \end{bmatrix} = \begin{bmatrix} 0 & -j \cos \alpha_2 & \sin \alpha_2 & 0 \\ -j \cos \alpha_2 & 0 & 0 & \sin \alpha_2 \\ \sin \alpha_2 & 0 & 0 & -j \cos \alpha_2 \\ 0 & \sin \alpha_2 & -j \cos \alpha_2 & 0 \end{bmatrix} \begin{bmatrix} \sin \alpha_1 \\ 0 \\ 0 \\ -j \cos \alpha_1 \end{bmatrix} \quad (2-22)$$

$$V_1' = 0 \quad (2-23)$$

$$V_2' = -j \cos \alpha_2 \sin \alpha_1 - j \sin \alpha_2 \cos \alpha_1 = -j \sin(\alpha_1 + \alpha_2) \quad (2-24)$$

$$V_3' = \sin \alpha_2 \sin \alpha_1 - \cos \alpha_2 \cos \alpha_1 = -\cos(\alpha_1 + \alpha_2) \quad (2-25)$$

$$V_4' = 0 \quad (2-26)$$

If $\alpha_1 = \alpha_2 = \frac{\pi}{8}$, $\sin\left(\frac{\pi}{8}\right) = 0.3827$ is the voltage coupling coefficient, which equals

$$-20 \log(0.3827) = 8.34 \text{ dB.}$$

Using these values of voltage coupling coefficients,

$$V_2' = -j \sin\left(\frac{\pi}{8} + \frac{\pi}{8}\right) = -j \sin\left(\frac{\pi}{4}\right) = -j\sqrt{1/2} \quad (2-27)$$

$$V_3' = -j \cos\left(\frac{\pi}{8} + \frac{\pi}{8}\right) = -j \cos\left(\frac{\pi}{4}\right) = -\sqrt{1/2} \quad (2-28)$$

which is equivalent to 3 dB coupling in terms of power.

Figure 2-11 shows a block diagram of such a coupler.

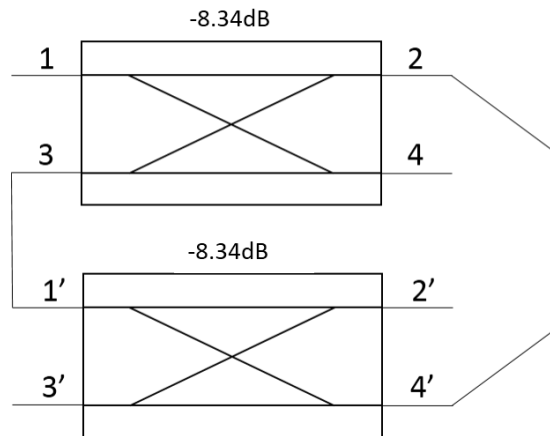


Figure 2-11 : 3 dB coupler as a tandem connection of two 8.34 dB couplers

2.4. Coupler Design

For this work, two multi-section 8.34 dB couplers are designed and then connected in tandem as discussed in the last section to achieve 3 dB or the hybrid coupler.

The theoretical design equations and tables given in [15] were used as reference for designing the 8.34 dB coupler. The work in [15] is based on finding an insertion loss function which is unity plus square of an odd polynomial function which follows from the previous work in [20]. Thus the theoretical design of a multi-section coupler reduces to finding the optimum polynomial function followed by extracting the even and odd-mode transmission-line impedances from the polynomial function. Following this analysis, theoretical values of odd and even mode impedances have been tabulated in [15] according to the required coupling coefficient, bandwidth and number of sections.

To minimize the area of design, least number of sections should be used. At the same time ultra-wideband operation must be achieved. The required bandwidth of 2-18 GHz was achieved for 8.34 dB coupler using a symmetric 7-section design having normalized even mode impedances 1.045, 1.122, 1.3014 and 2 Ohms. For a 50 Ohm design, these are multiplied by 50 to get the even mode impedance to be realized. Odd mode impedance can be calculated using [21],

$$Z_0^2 = Z_{0e} Z_{0o} \quad (2-29)$$

Where $Z_0 = 50$ Ohms, Z_{0e} and Z_{0o} are even and odd mode impedances respectively.

The voltage coupling coefficient is given by, $\frac{Z_{0e} - Z_{0o}}{Z_{0e} + Z_{0o}}$ which is equivalent to

$20 \log \left(\frac{Z_{0e} - Z_{0o}}{Z_{0e} + Z_{0o}} \right)$ in dB. Using these equations even mode impedances for the symmetric 7-section design are found to be 52.27, 56.10, 65.07 and 107.82 Ohms and the odd mode impedances are 47.83, 44.56, 38.42 and 23.19 Ohms. The coupling factors are 27.06 dB, 18.81 dB, 11.78 dB and 3.80 dB.

The 3.80 dB tight coupling is still hard to realize as edge coupled microstrip lines as discussed in previous sections. Hence homogenous stripline structure has been designed which also helps in maintaining equal odd and even mode phase velocities since pure TEM mode propagates. The center section which requires tight coupling of 3.80 dB is designed as broadside coupled since it provides large area for coupling and other six sections are designed as offset coupled. The geometries of broadside and offset coupled striplines were shown in **Figure 2-1**.

The geometry of each section of stripline is decided according to the coupling required. For broadside coupled striplines the even and odd mode characteristic impedances are given by [22] (assuming negligible strip thickness),

$$Z_{0e} = \frac{60\pi}{\sqrt{\epsilon_r}} \frac{K'(k)}{K(k)} \quad (2-30)$$

$$Z_{0o} = \frac{296.1}{\sqrt{\epsilon_r} \frac{b}{s} \tanh^{-1}(k)} \quad (2-31)$$

where K is complete elliptic function of the first kind, and K' is the complementary function given by,

$$K'(k) = K(k') = K(\sqrt{1 - k^2}) \quad (2-32)$$

where k is related to the dimensions of the structure as follows:

$$\frac{W}{b} = \frac{1}{\pi} \left[\ln \left(\frac{1+R}{1-R} \right) - \frac{S}{b} \ln \left(\frac{1+R/k}{1-R/k} \right) \right] \quad (2-33)$$

$$R = \left[\left(k \frac{b}{S} - 1 \right) / \frac{1}{k} \frac{b}{S} - 1 \right]^{1/2} \quad (2-34)$$

where, b , W , S are shown in **Figure 2-1** (c).

For voltage coupling coefficient, C and terminal characteristic impedance Z_0 , the odd even mode characteristic impedance is be given by [19],

$$Z_{0e} = Z_0 \left(\frac{1+C}{1-C} \right)^{1/2} \quad (2-35)$$

$$Z_{0o} = Z_0 \left(\frac{1-C}{1+C} \right)^{1/2} \quad (2-36)$$

and,

$$\frac{K}{K'} = \frac{60\pi}{Z_0 \sqrt{\epsilon_r}} \left(\frac{1-C}{1+C} \right)^{1/2} \quad (2-37)$$

[23] presented formulas for K/K' can be used to calculate k for given coupling and substrate.

$$\frac{K}{K'} = \frac{1}{\pi} \ln \left(2 \frac{1+\sqrt{k}}{1-\sqrt{k}} \right) \quad \text{for } 0.707 < k < 1 \quad (2-38)$$

$$\frac{K}{K'} = \frac{\pi}{\ln \left(2 \frac{1+\sqrt{k'}}{1-\sqrt{k'}} \right)} \quad \text{for } 0.0 < k < 0.707 \quad (2-39)$$

For $K/K' > 1$ or $C < (1.0 - P\epsilon_r)/(1.0 + P\epsilon_r)$, k is expressed as,

$$k = \left(\frac{0.5 e^{(\pi K/K')} - 1}{0.5 e^{(\pi K/K') - 1}} \right)^2 \quad (2-40)$$

And for the case of $K/K' < 1$ or $C > (1.0 - P\epsilon_r)/(1.0 + P\epsilon_r)$, k is expressed as,

$$k = \left[1 - \left(\frac{0.5 e^{(\pi K'/K)} - 1}{0.5 e^{(\pi K'/K) - 1}} \right)^4 \right]^{1/2} \quad (2-41)$$

where $P = (Z_0/60\pi)^2$ and in the geometry the ratio,

$$\frac{S}{b} = 0.0017 Z_0 \sqrt{\epsilon_r} \left(\frac{1-C}{1+C} \right)^{1/2} \ln \frac{1+k}{1-k} \quad (2-42)$$

These elliptical integrals can also be evaluated in Python. For given C , ϵ_r and Z_0 the geometry ratios W/b and S/b can be calculated using these equations. Stripline calculators can also be used to instead of solving these equations.

Analysis for offset coupled lines has been given in [24], which is skipped because modern stripline calculators can be used to find the geometries of the coupled lines according to the coupling requirement or the even and odd mode impedances.

Although the tables and equations can theoretically design any coupler but for a physically realizable structure the spacing ' s ' in **Figure 2-1** should be uniform throughout for each section and at the same time the widths ' w ' and spacing ' w_c ' should not be too large or too small. Such constraints were satisfied by diligently selecting substrate type and designing the stripline structure. Duroid 4003 ($\epsilon_r = 3.55$) is used as substrate in this work which satisfied the above constraints. Using equations mentioned in this section, even odd mode impedances are calculated for each section and using the equations or calculators the geometry of each section was calculated for Duroid 4003.

Figure 2-12 shows the designed 7-section symmetric 8.34 dB coupler, with center section as broadside coupled and the 6 sections as offset coupled striplines. Magnitude and phase response is shown in **Figure 2-14**. **Figure 2-13** highlights the generic stripline structure that will be followed for all the further designs discussed in this thesis.

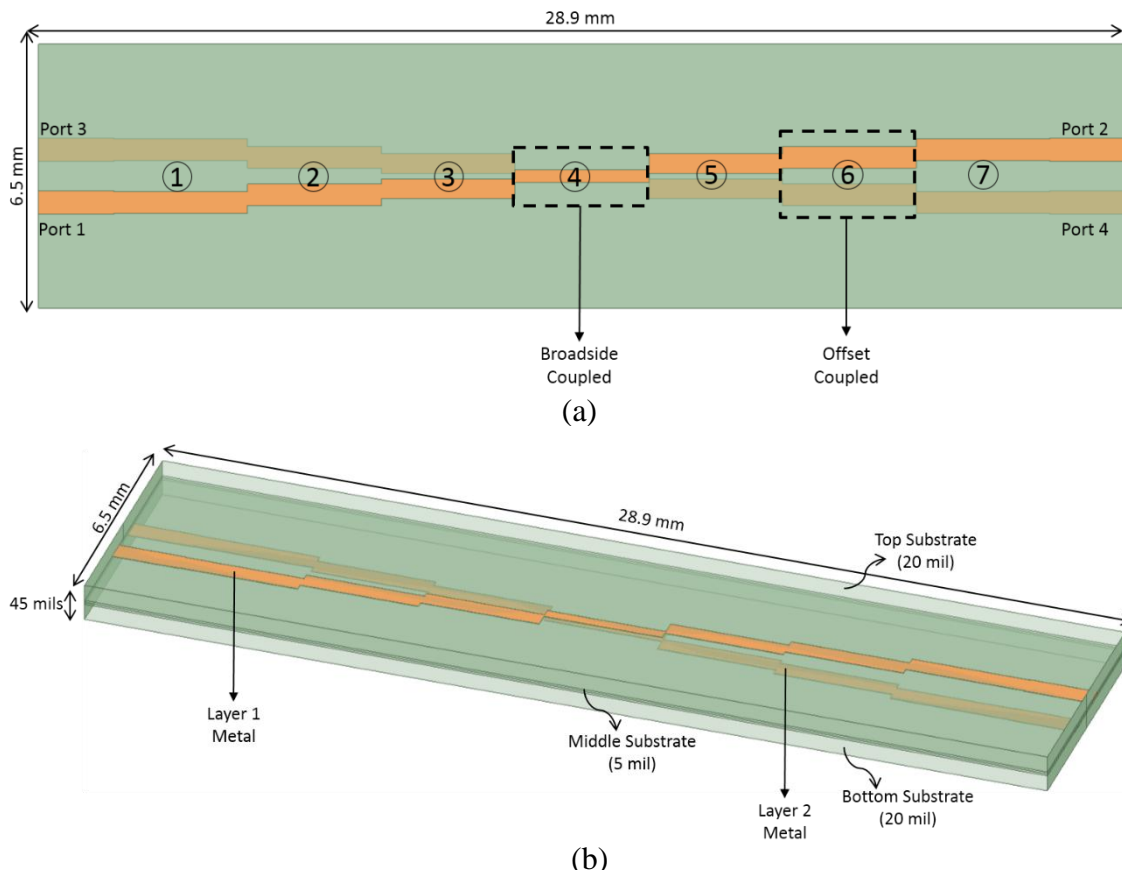


Figure 2-12 : 7-section 8.34 dB stripline coupler (a) Top view (b) Trimetric view

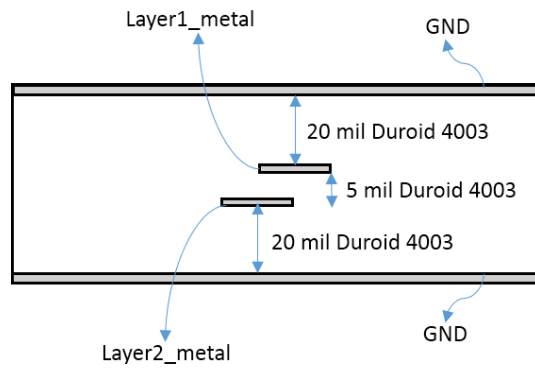
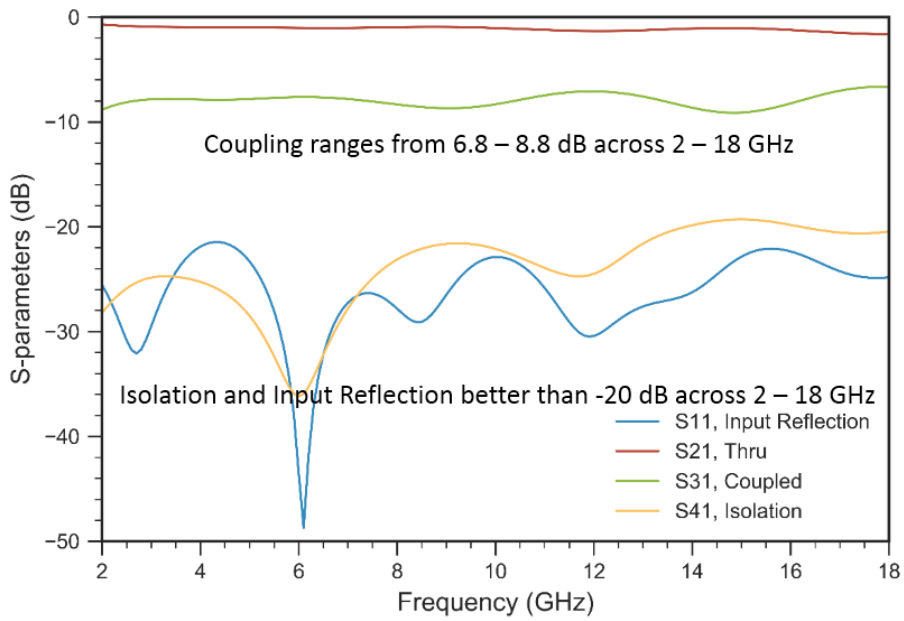
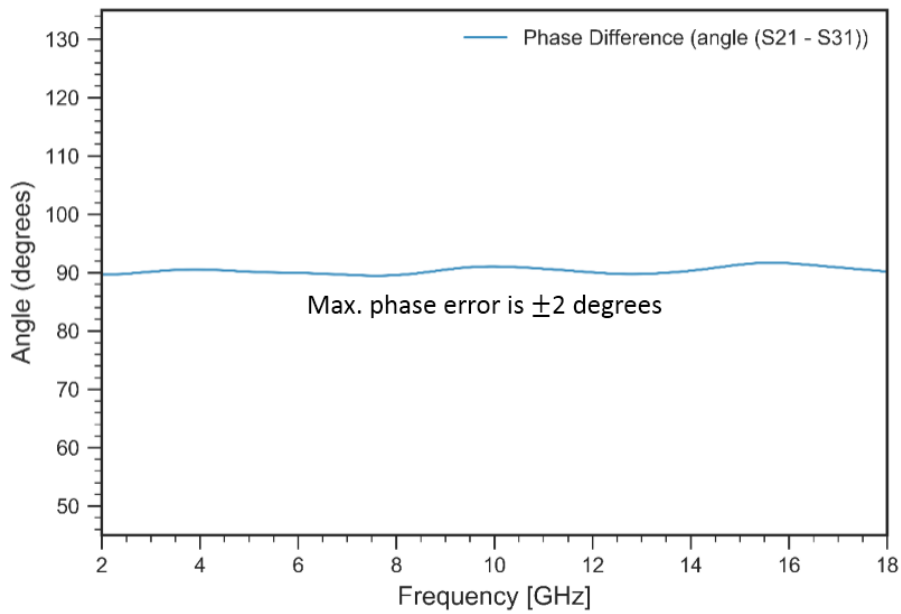


Figure 2-13 : Geometry of stripline structures



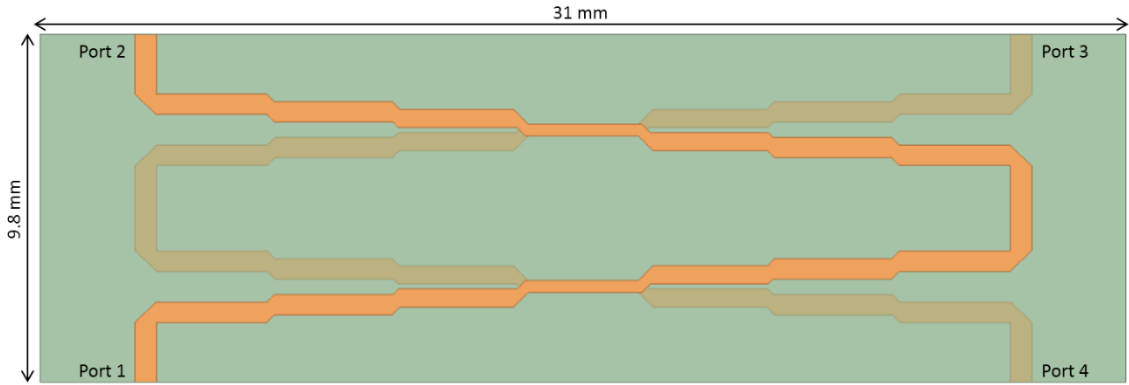
(a)



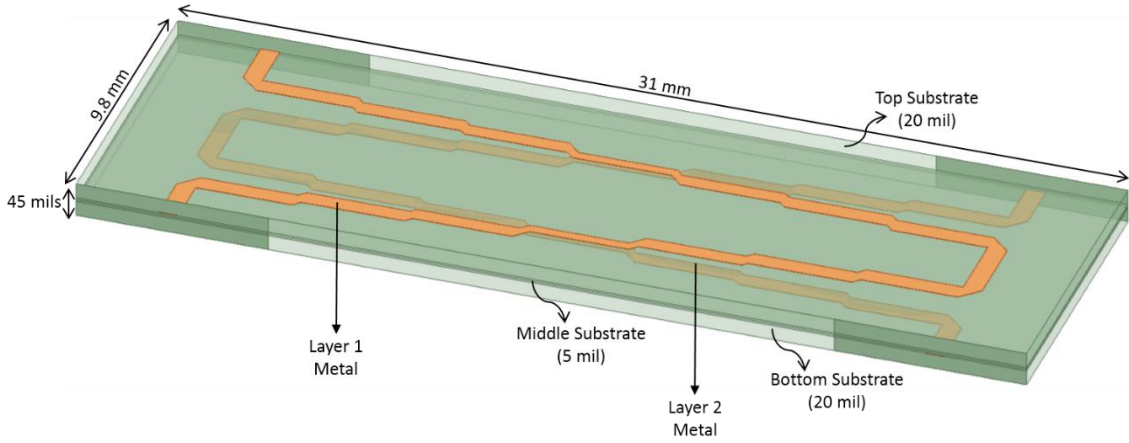
(b)

Figure 2-14 : Magnitude and phase response of 7-section 8.34 dB coupler (a) Magnitude response (b) Phase response

As discussed in last subsection two 8.34 dB couplers connected in tandem result in 3 dB coupler. **Figure 2-15** is the designed 3 dB coupler by connecting the above 8.34 dB couplers.

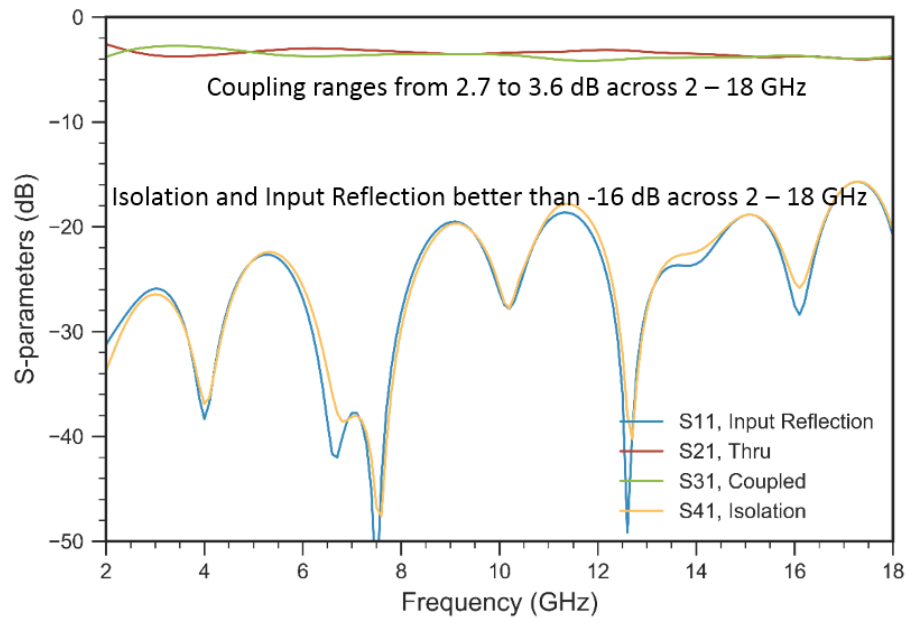


(a)

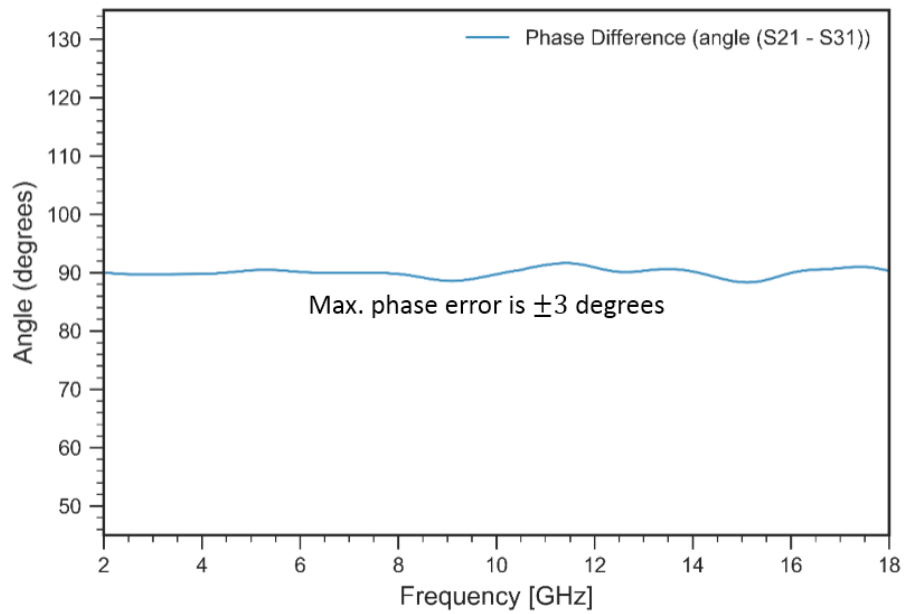


(b)

Figure 2-15 : 3 dB coupler as a tandem connection of two 8.34 dB couplers (a) Top view (b) Trimetric view



(a)



(b)

Figure 2-16 : Magnitude and phase response of 3 dB coupler
(a) Magnitude response (b) Phase response

Figure 2-16 (a) shows it achieves tight coupling varying from 2.5 dB to 3.6 dB across 2-18 GHz range. **Figure 2-16 (b)** shows the phase difference between the through and coupled ports which is 90° with an error of $\pm 3^\circ$.

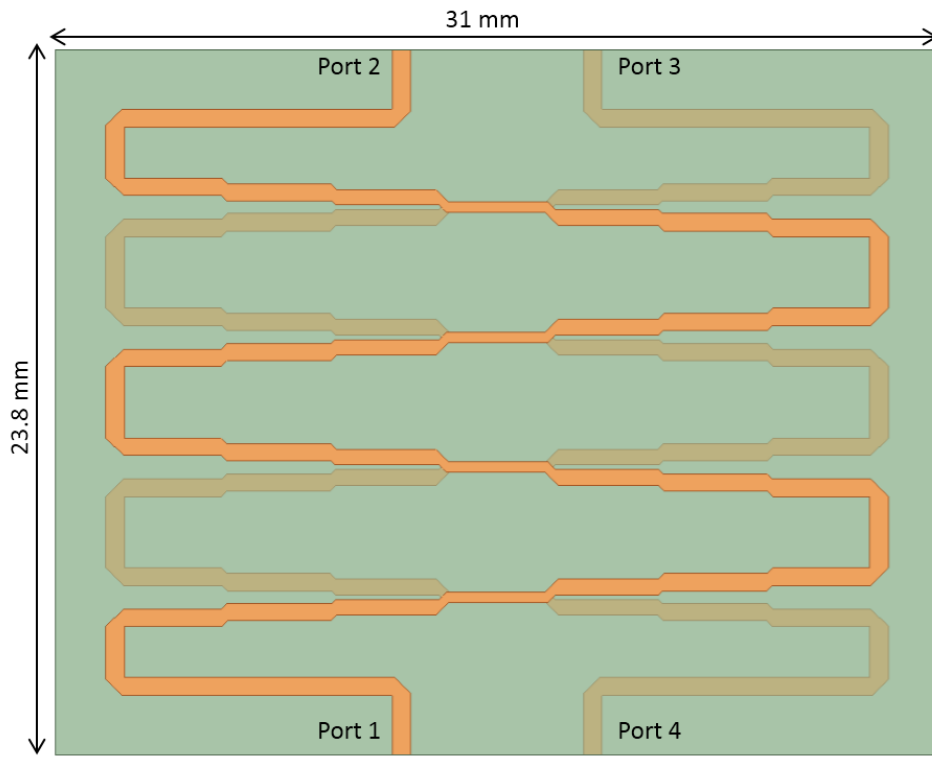
Similar coupler was designed in [25], with 41 sections (97 mm x 46 mm) for 0.5-18 GHz. The simulated results in [25] show coupling lowers as the frequency increases, with 5 dB coupling at 18 GHz. In this work tight coupling (2.6 dB to 3.7 dB) is achieved for 2-18 GHz with much smaller size (31.78 mm x 9.78 mm).

3. CROSSOVER DESIGN

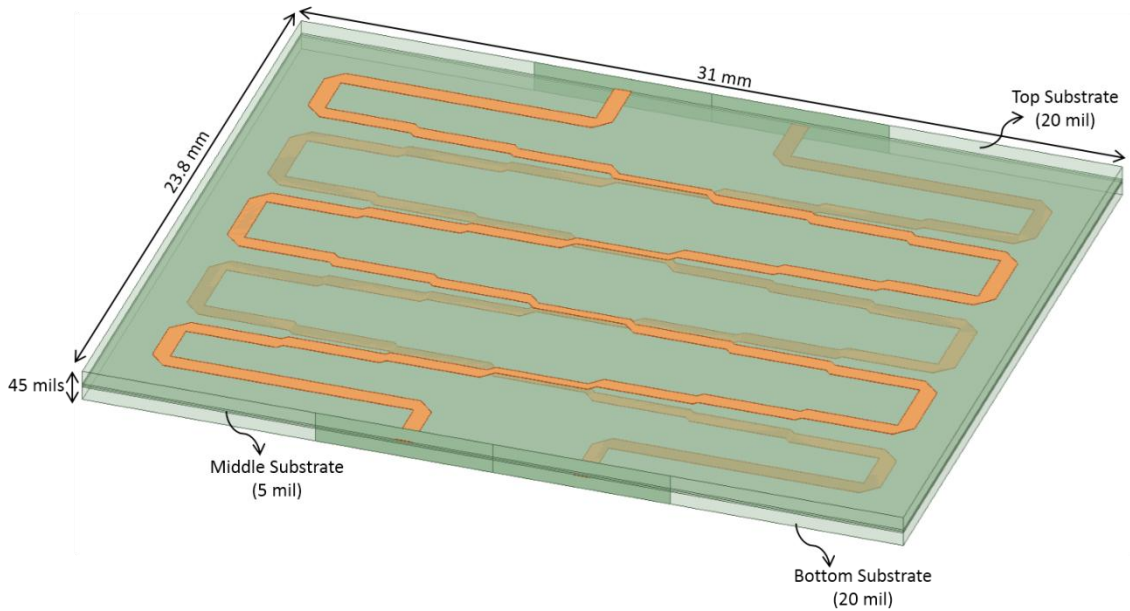
This brief section covers the design of crossover required for Butler Matrix. As discussed in Section 1.3 crossover is designed by connecting two 3 dB couplers in tandem. **Figure 3-1** shows such a crossover design in HFSS. Extra line lengths are added to assist in layout of Butler Matrix later.

Although the physical size of the crossover is small, but the electrical size is too large considering the highest frequency of operation is 18 GHz. Moreover the simulations need to run from 2 to 18 GHz to analyze the design over the full bandwidth. For running finite element method simulations in HFSS, such a design requires large computational resources. Therefore these simulations were run on supercomputing cluster, Texas A&M High Performance Research Computing (HPRC).

Figure 3-2 shows its magnitude response. Ideally all the input power should be present at output but due to long length of transmission lines we see maximum insertion loss of -2.6 dB.



(a)



(b)

Figure 3-1 : Crossover design as a tandem connection of two 3 dB couplers (a) Top View (b) Trimetric View

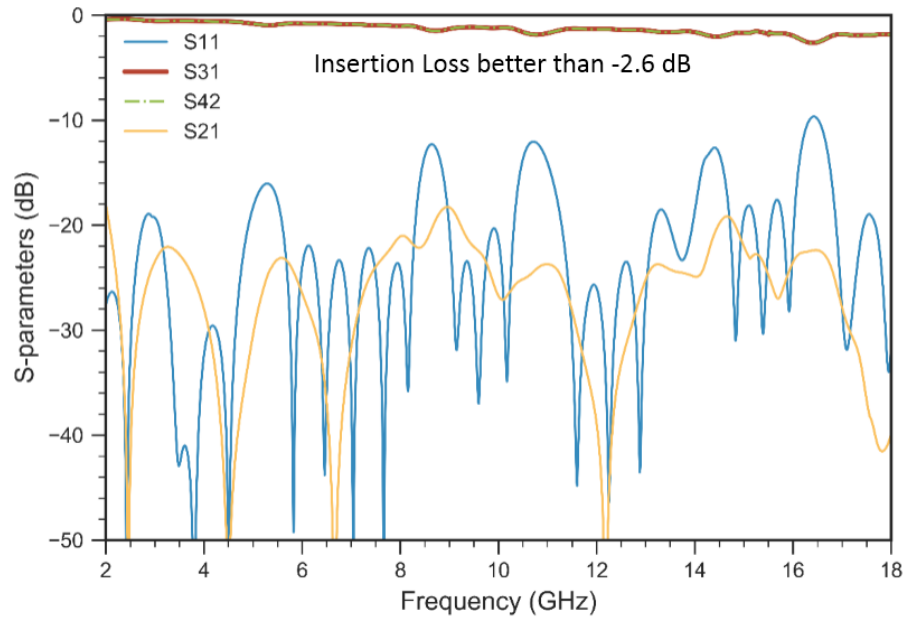


Figure 3-2 : Crossover magnitude response

4. PHASE SHIFTER DESIGN

As discussed in Section 1.1 a 4x4 Butler Matrix requires 45 degree phase shifters. For a narrow band design such a phase shift was easily obtained by designing a transmission line which is electrically 45 degrees longer than a reference line. Although it is a quick way to achieve phase shift, it cannot provide a flat phase shift over a very broad range of frequencies.

To achieve a flat phase shift over a wide bandwidth, a class of differential phase shifter called Schiffman phase shifter [26] was designed. These are four port circuits and provide a constant differential phase shift across the two output ports over a frequency range. Schiffman proposed a design of phase shifter shown in **Figure 4-1**, which consists of two TEM transmission lines. One of the lines is the reference line and the other is a pair of parallel coupled transmission lines connected at one end. Length of this connection is kept as small as possible. This pair of parallel coupled lines is also called a single C-section. The parallel coupled lines are each a quarter-wavelength long at the center/design frequency. The reference line is just a straight TEM line, which in the case of Butler Matrix would be the crossover discussed in last section.

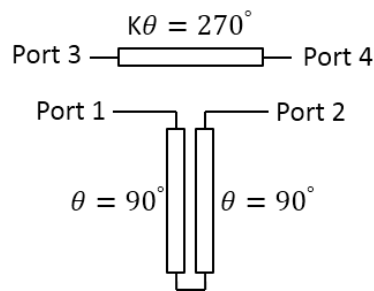


Figure 4-1 : Schiffman phase shifter

Following expressions given by [21] determine the characteristic impedance and phase response of the Schiffman coupled section, in terms of even and odd mode impedances and the electrical line length,

$$Z_0^2 = Z_{0e} Z_{0o} \quad (4-1)$$

$$\cos \phi = \frac{\rho - \tan^2 \theta}{\rho + \tan^2 \theta} \quad (4-2)$$

where,

$$\rho = \frac{Z_{0e}}{Z_{0o}} \quad (4-3)$$

and θ is the electrical length of the each of the coupled line.

The parameter ρ is also related to coupling C , in dB,

$$C = -20 \log \left(\frac{\rho - 1}{\rho + 1} \right) \quad (4-4)$$

The total phase shift is equal to the phase difference ($\Delta\phi$) between the reference line and the single C-section coupled lines. Thus,

$$\Delta\phi = K\theta - \cos^{-1} \left(\frac{\rho - \tan^2 \theta}{\rho + \tan^2 \theta} \right) \quad (4-5)$$

$K\theta$ is the transmission phase of the reference line.

There are a number of design parameters such as $K, \theta, Z_{0e}, Z_{0o}$. Further, the product of even and odd mode impedances and their ratio ρ can be fixed independently. Thus the characteristic impedance Z_0 of the coupled line network can be specified independent of phase response ϕ . Once the desired phase response ϕ , or the total phase shift $\Delta\phi$, is specified the Schiffman phase shifter can be designed with different values of Z_{0e}, Z_{0o} and θ . It has been shown in [27] that if at the center frequency, length of each of

the coupled line equals quarter wavelength or $\theta = \pi/2$, then the phase shift $\Delta\phi$ is anti-symmetric around the center frequency, which leads to the broadest bandwidth.

Figure 4-2 shows the phase shift for 90 degree Schiffman phase shifters designed using different values odd, even mode impedances and coupling values while keeping the product, $Z_0^2 = Z_{0e} Z_{0o}$ constant and equal to 50 Ohms. Different values of the ratio ρ yields varying bandwidths. For the designs with higher bandwidth the deviation in phase response or the error is also higher. A bandwidth of 1.95:1 was reported in [26] with a phase shift of 90 ± 2.5 degrees for $\rho = 2.7$. Bandwidth of 2.34:1 was achieved for phase shift of 90 ± 4.8 degrees.

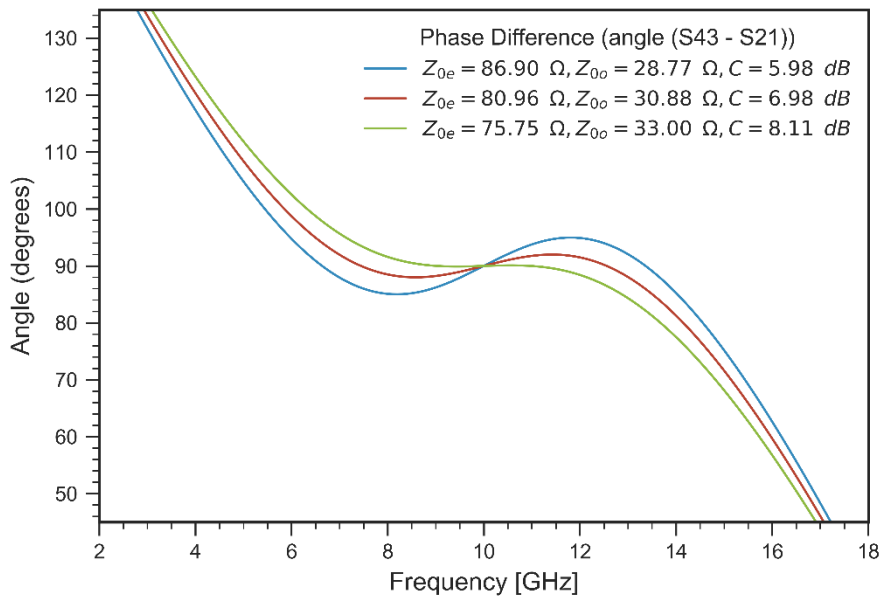


Figure 4-2 : Phase response of single section 90° Schiffman phase shifters

For ultra-wideband design of the Butler matrix, bandwidth requirement is 9:1 (2-18GHz). The single C-section Schiffman phase shifter can be extended to multiple

sections of coupled lines to increase bandwidth over which the phase shift is flat.

Analysis for this was done in [28]. The equations extend from the phase response of the single section. For 'n' sections of coupled line in a Schiffman phase shifter the phase response is given by,

$$\cos \phi_n = \frac{\rho_1 - \tan^2 \theta'_1}{\rho_1 + \tan^2 \theta'_1} \quad (4-6)$$

where,

$$\theta'_1 = \theta_1 + \tan^{-1}(\rho_{12} \tan \theta'_2) \quad (4-7)$$

$$\theta'_2 = \theta_2 + \tan^{-1}(\rho_{23} \tan \theta'_3) \quad (4-8)$$

.

.

$$\theta'_{n-1} = \theta_{n-1} + \tan^{-1}(\rho_{n-1,n} \tan \theta'_n) \quad (4-9)$$

$$\theta'_n = \theta_n \quad (4-10)$$

and

$$\rho_{i,i+1} = \frac{Z_{0e i}}{Z_{0e (i+1)}} = \frac{Z_{0o (i+1)}}{Z_{0o i}} \quad (4-11)$$

While $Z_0^2 = Z_{0e i} Z_{0o i}$ is true for each section.

As in the case of multi-section hybrid coupler, the equations result in a theoretical design which may or may not be physically realizable. Using the same substrate as before Duroid 4003 ($\epsilon_r = 3.55$), a 5-section 45 degree phase shifter was designed diligently to provide a constant phase shift over 2 to 18 GHz. **Figure 4-3** shows the initial design of 5-section Schiffman phase shifter. A straight transmission line is used as reference. To shorten the simulation time, the straight line was designed to be short but extra length added to it in terms of de-embed as shown in **Figure 4-44**. **Figure 4-5** shows the constant 45 degree phase shift with an error of $\pm 5^\circ$.

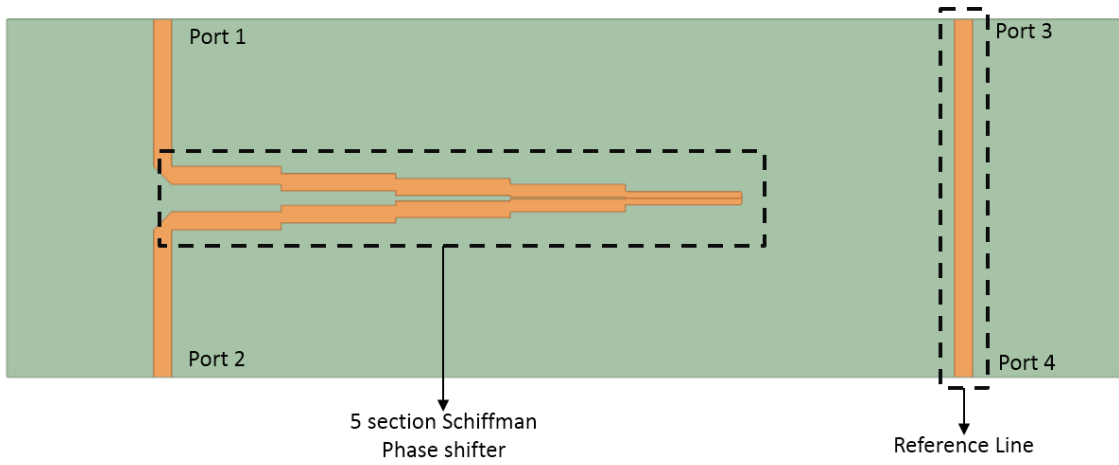


Figure 4-3 : 5-section Schiffman phase shifter with a straight reference line

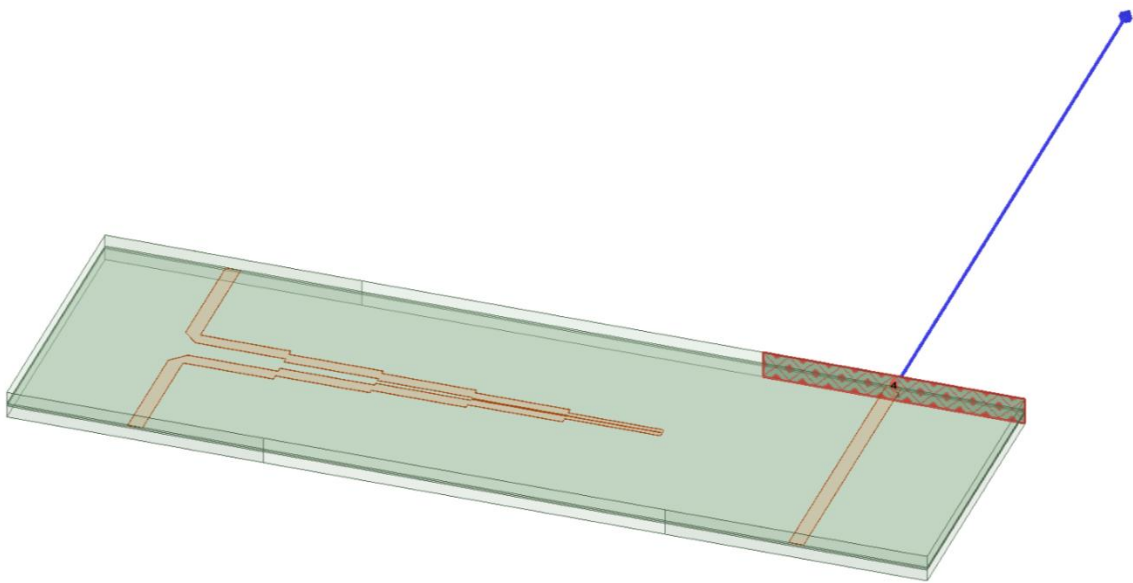


Figure 4-4 : Schiffman phase shifter with reference line showing the de-embed

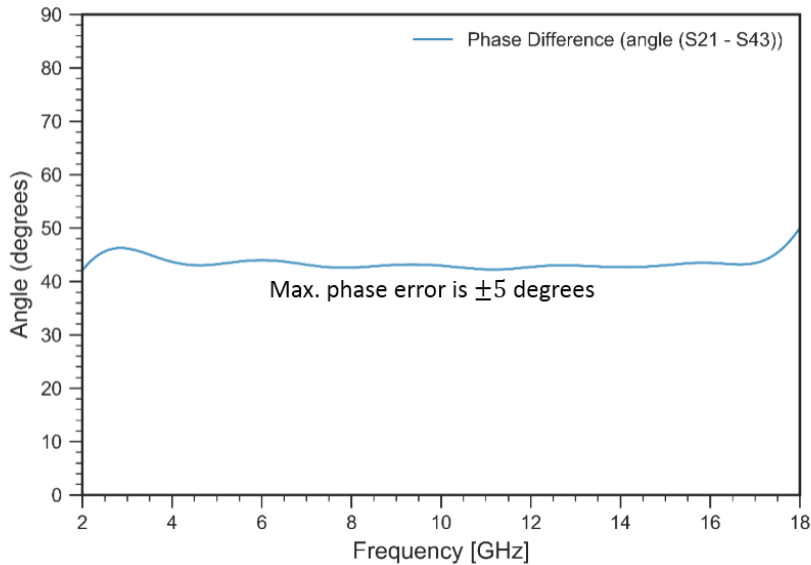


Figure 4-5 : Phase response of 5-section 45 degrees Schiffman phase shifter with respect to a straight line

In the Butler matrix design the reference line is not a straight line, rather it's the crossover and any extra line lengths that are added due to the layout. Therefore the phase shifter design was modified accordingly and added extra lengths were added to match the slope of phase response of the crossover. **Figure 4-66** shows the design of such a phase shifter with crossover. The phase shift is 45 degrees with maximum error of $\pm 7^\circ$ as shown in **Figure 4-77**.

A 6-section phase shifter was also design to flatten the phase shift even more and hence reduce the error. The phase response of such a phase shifter is shown in **Figure 4-88** it didn't significantly reduce the phase error, but there was an improvement of 1° .

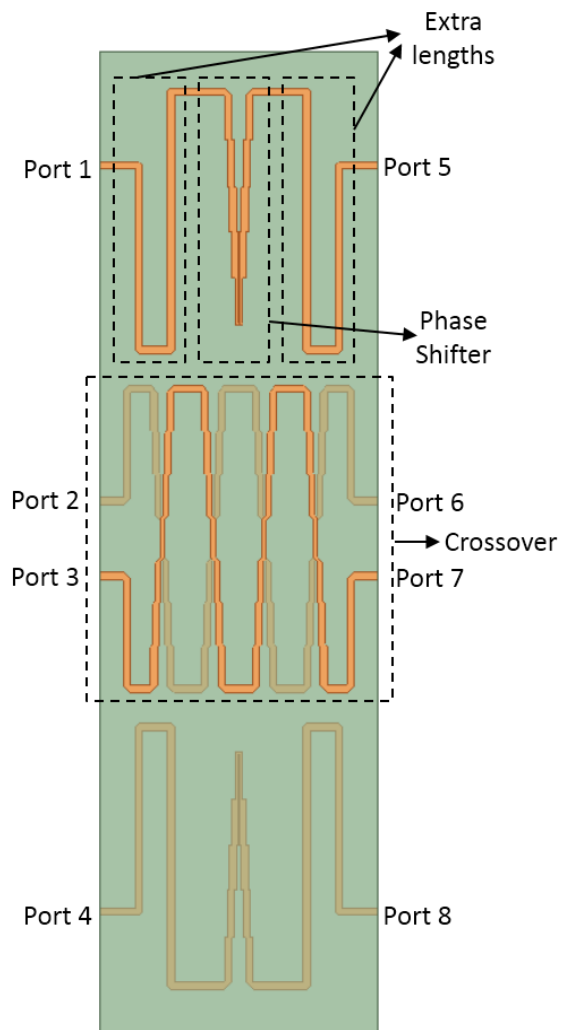


Figure 4-6 : Phase shifter with extra lengths to compensate for crossover phase response

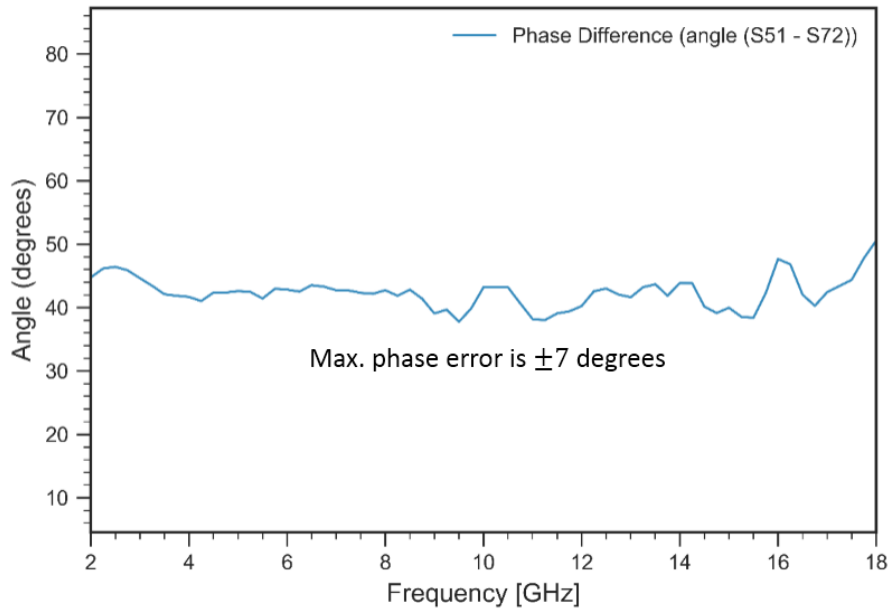


Figure 4-7 : Phase response of 5-section 45 degrees Schiffman phase shifter with respect to crossover

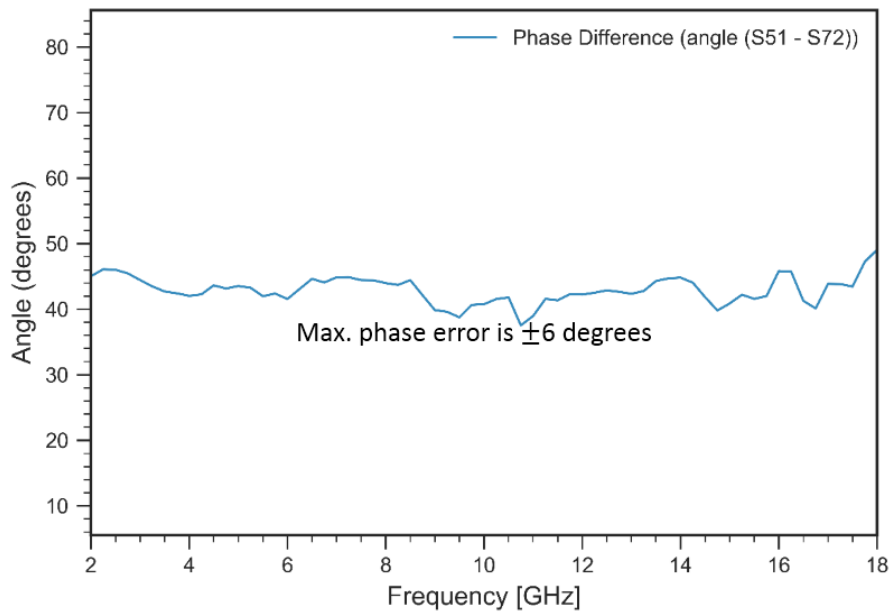


Figure 4-8 : Phase response of 6-section 45 degrees Schiffman phase shifter with respect to crossover

Using the same design procedure two more phase-shifters were designed. These are 22.5 degrees and 67.5 degrees phase shifters for the design of 8-input, 8-output (8x8) Butler matrix. A schematic of 8x8 Butler matrix was shown in **Figure 1-3**. Phase response of these phase shifters are shown in **Figure 4-9** and **Figure 4-10**. As with the case of 45 degree phase shifter, there are some errors amounting upto $\pm 8^\circ$.

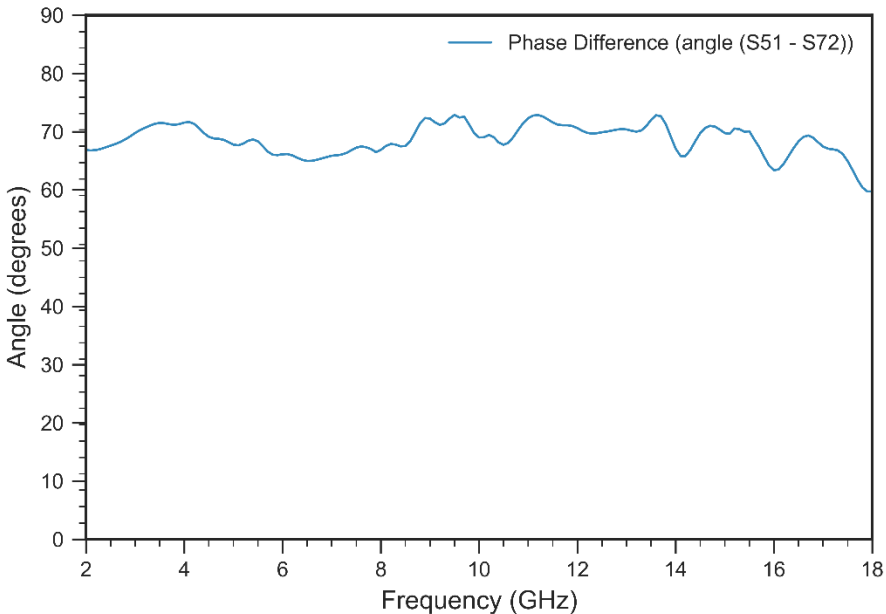


Figure 4-9 : Phase response of 6-section 67.5 degrees Schiffman phase shifter with respect to crossover

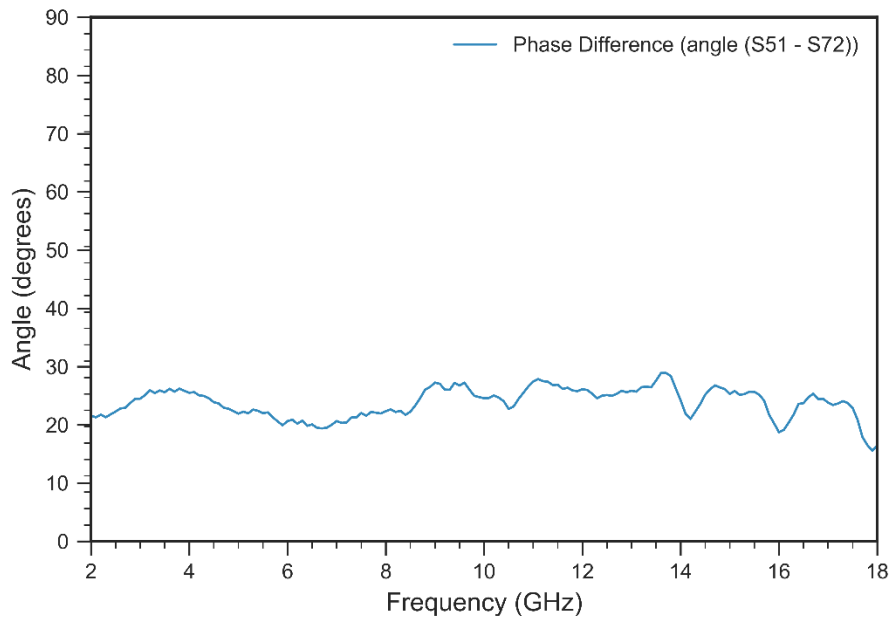


Figure 4-10 : Phase response of 6-section degrees Schiffman phase shifter with respect to crossover

5. 4X4 BUTLER MATRIX DESIGN AND RESULTS

The previous three sections described the design and results of the three building blocks of the ultra-wideband butler matrix, hybrid coupler, crossover and a phase shifter. Comparing the block diagram of **Figure 1-2** and the design in **Figure 4-6** it's only a matter of adding the four hybrid couplers to get to the design of Butler matrix. **Figure 5-1** and **Figure 5-2** show the complete layout/design of ultra-wideband 4-input, 4-output Butler Matrix. It uses the 3-dB coupler designed as a tandem connection of two 7-section 8.34 dB hybrid couplers, the crossover and 6-section 45 degrees phase shifters. It follows the same general structure as shown in. **Figure 2-13**.

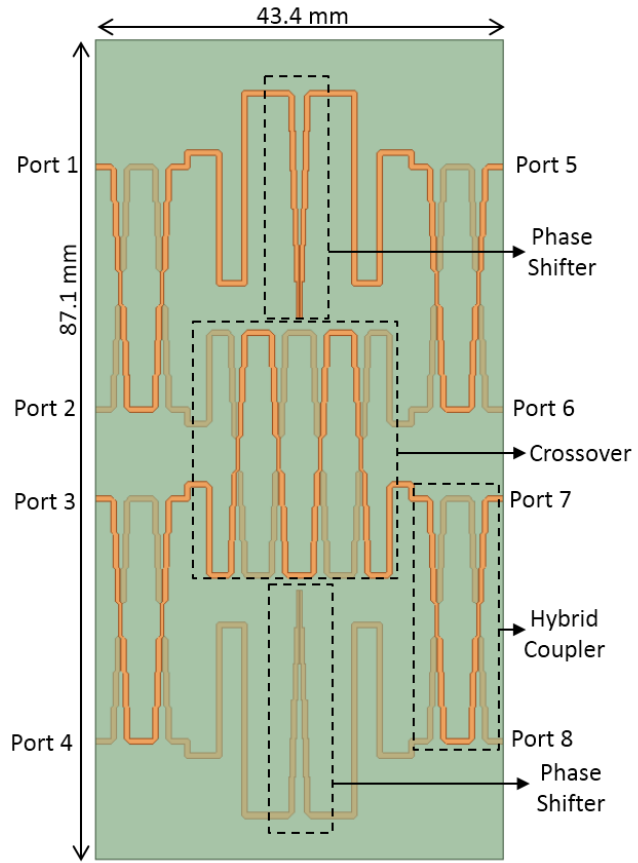


Figure 5-1 : Layout of 4x4 ultra-wideband Butler matrix (Top View)

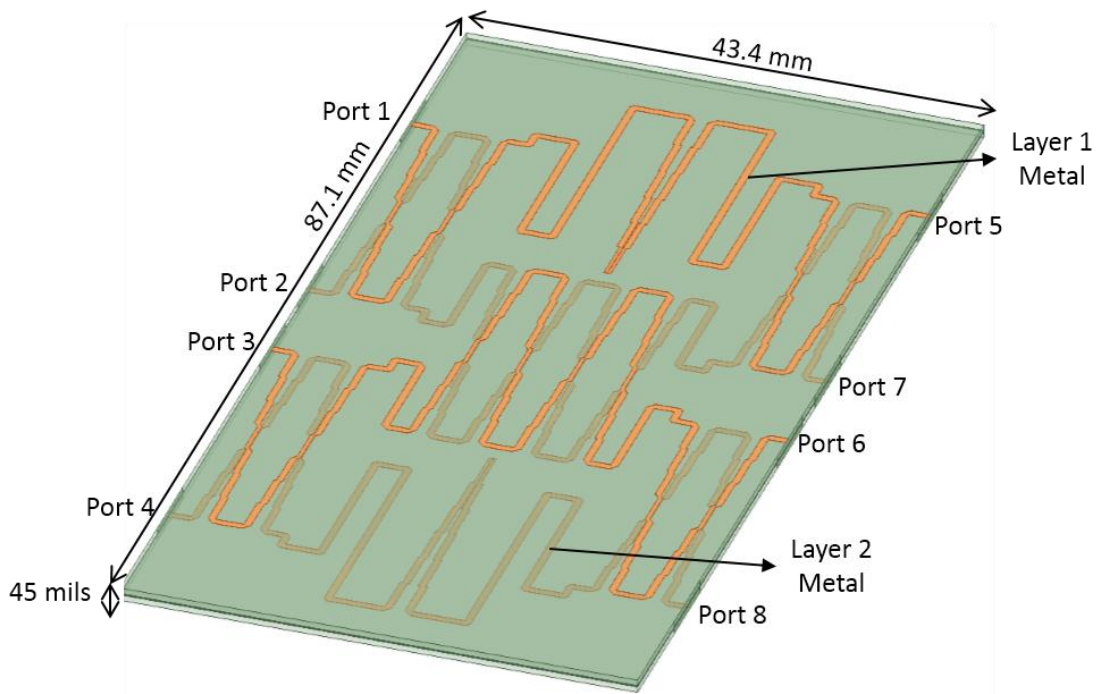


Figure 5-2 : Layout of ultra-wideband Butler matrix (Trimetric view)

Figure 5-3 and **Figure 5-4** show the magnitude response with input at Port 1 and Port 2 respectively. Power is equally distributed among all the output ports. The insertion loss is more at higher frequencies. Due to long lengths of transmission lines from each input to the output port we see a high insertion loss. Phase response is shown in **Figure 5-5** and **Figure 5-6**. With respect to Port 1 we see a progressive phase shift of 45 degrees and 135 degrees with respect to Port 2. The phase errors have accumulated in the complete design and as a result, at a few frequency points the errors reach $\pm 15^\circ$. But the phase shifts are centered at 45 degrees and 135 degrees for the entire frequency range from 2-18 GHz. Since the Butler matrix is symmetrical and the layout is also symmetrical the magnitude and phase response for Port 3 and Port 4 are also similar, with progressive phase shifts of -135 degrees and -45 degrees respectively.

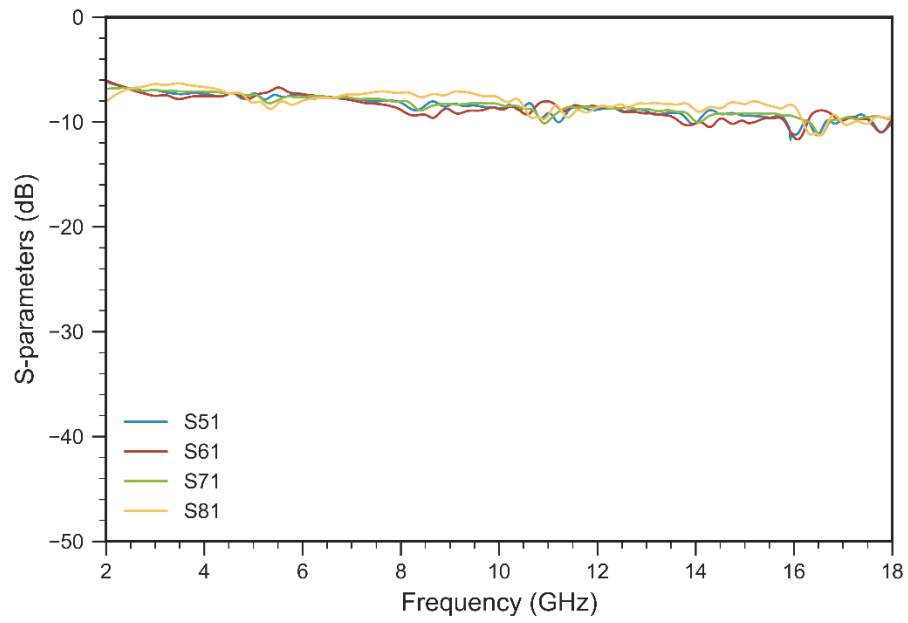


Figure 5-3 : Magnitude Response of Butler matrix with respect to Port 1

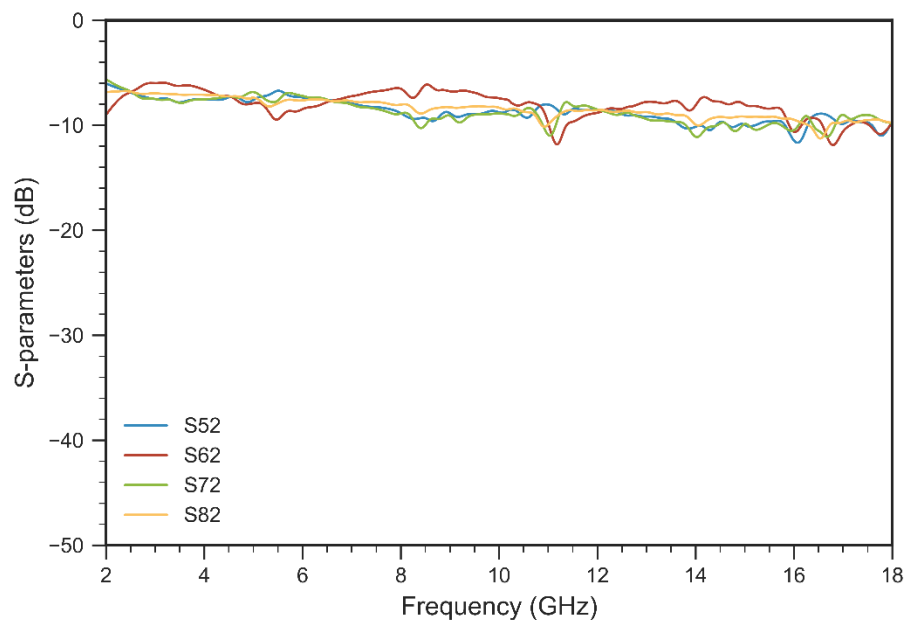


Figure 5-4 : Magnitude response of Butler matrix with respect to Port 2

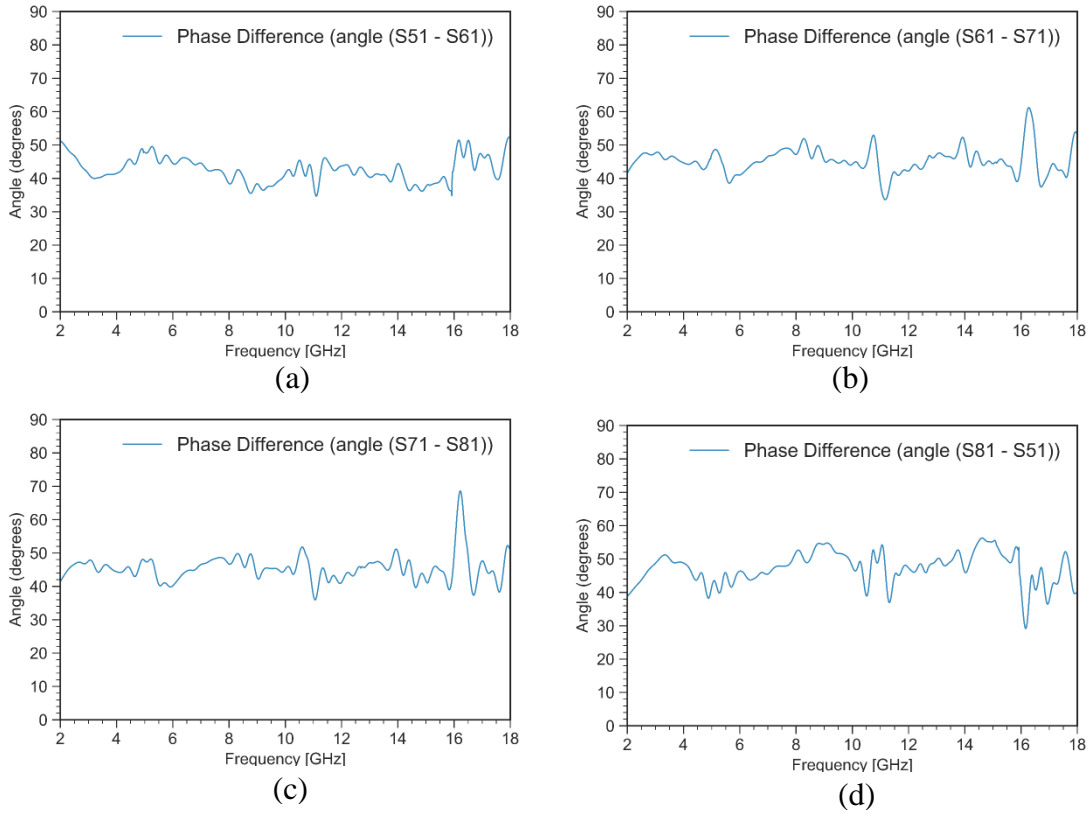


Figure 5-5 : Butler Matrix progressive phase shifts of 45° with respect to Port 1

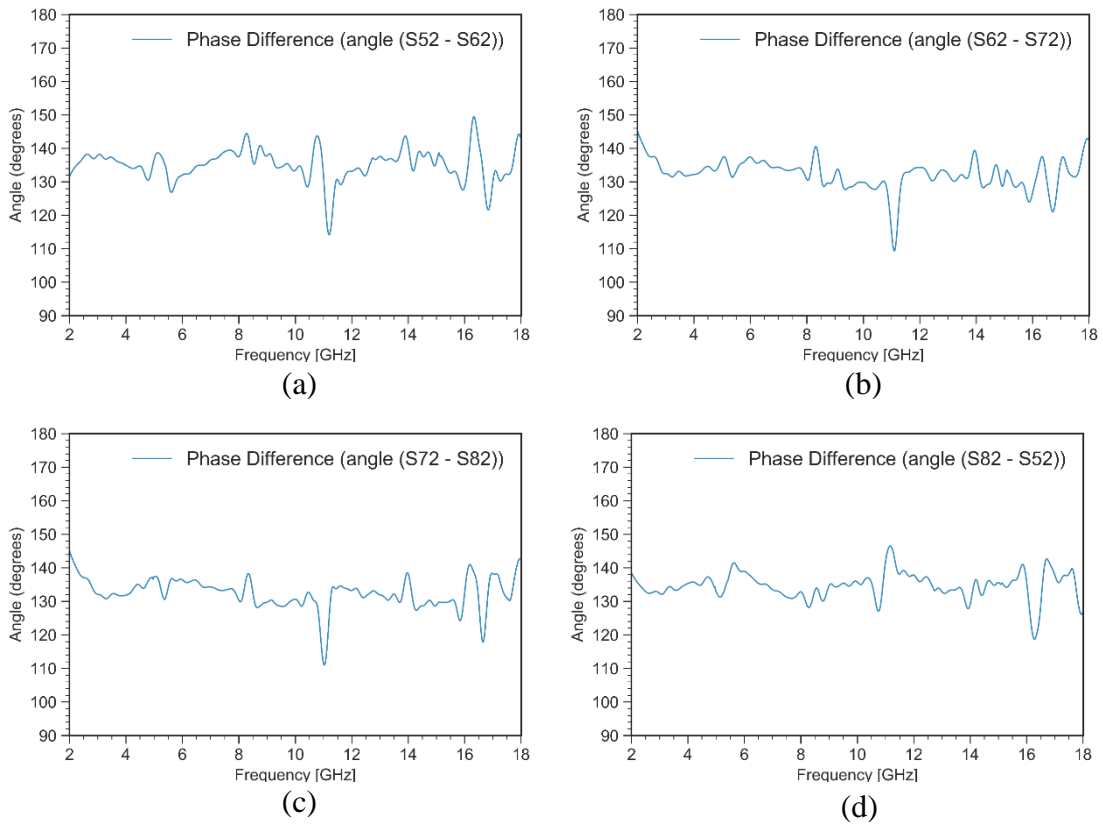


Figure 5-6 : Butler Matrix progressive phase shifts of 135° with respect to Port 2

6. FUTURE WORK

6.1. TRL Calibration Kit

Once fabricated, the above designed circuits would require de-embedding techniques for measurement with VNA. This subsection covers the design of TRL (Through – Reflect - Line) calibration kit for measurement across 2-18 GHz. Only two-port kits have been designed. Through is designed as just back to back connection of the ports shown in **Figure 6-1**. Reflect standard can be designed as open or short. In this case it has been designed as short, by connecting the stripline with the ground planes at top and bottom as shown in **Figure 6-2**.

Since the circuits in this work are ultra-wideband (2-18 GHz), having a bandwidth ratio of 9:1, two Line standards have been designed. One has length equal to quarter wavelength at 6 GHz and the other at 14 GHz as shown in **Figure 6-3**.

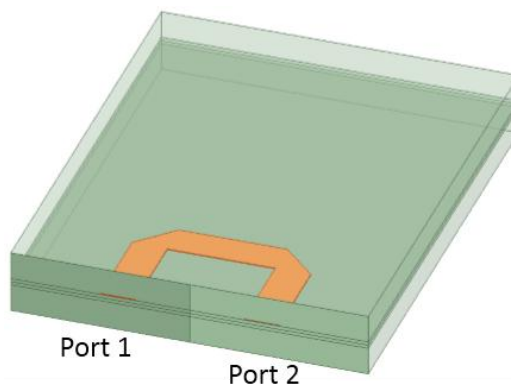


Figure 6-1 : Through standard

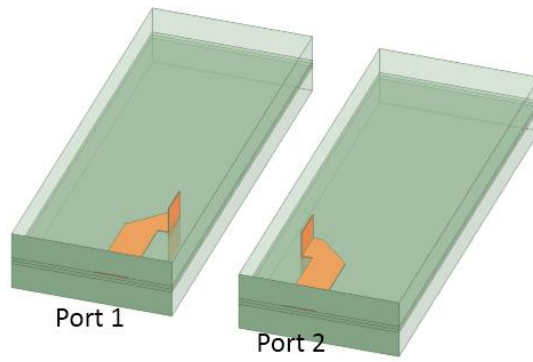
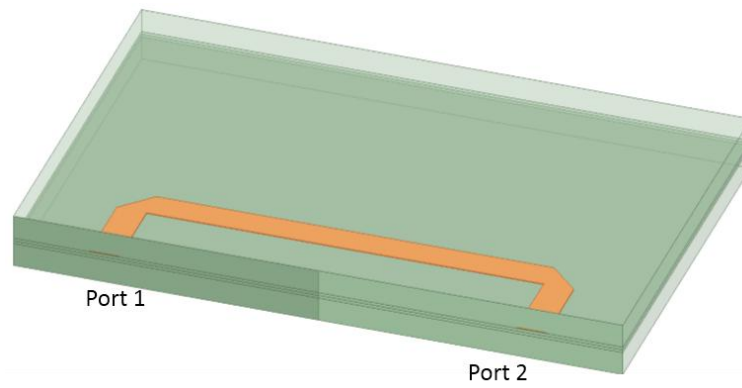
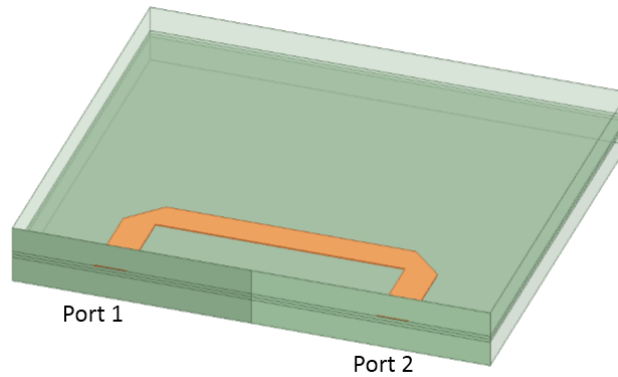


Figure 6-2 : Reflect standard



(a)



(b)

Figure 6-3 : Line standards

(a) Quarter-wavelength long at 6 GHz (b) Quarter-wavelength long at 14 GHz

For verification, that the designed TRL calibration kit works, two-port magnitude data of the designed 3 dB coupler is compared with and without the TRL kit. This can be done quickly in Python using scikit-rf library. As can be seen from **Figure 6-44** and **Figure 6-55**, the application of calibration kit does not affect the two-port response of the coupler appreciably. Hence the designed calibration kit can be used for measurement.

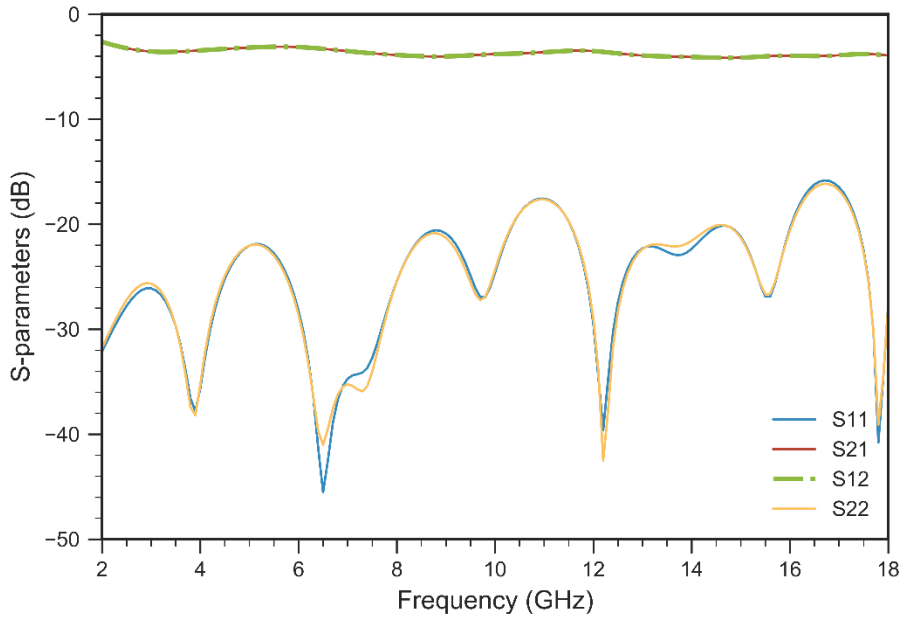


Figure 6-4 : Two-port response of hybrid coupler without calibration kit

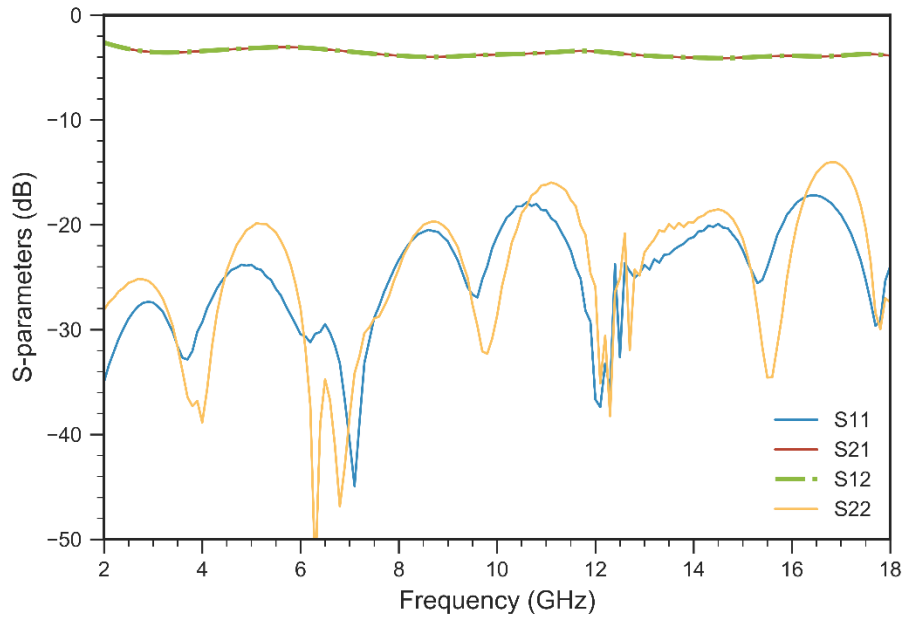


Figure 6-5 : Two-port response of hybrid coupler with calibration kit

6.2. 8X8 Butler Matrix

The block diagram of 8-input, 8-output (8x8) Butler matrix was shown in **Figure 1-3**. Each of the building blocks of the 8x8 Butler matrix, i.e., hybrid coupler, crossover, 22.5 degrees and 67.5 degrees phase shifter has been designed in this work.

Unfortunately the full layout of 8x8 Butler matrix is electrically too large, which make its analysis a long process. For instance one instance of FEM simulation for the 4x4 Butler matrix takes around a week to run. An 8x8 Butler matrix being electrically large would take even more time for a single simulation.

Another task before moving onto the design of 8x8 Butler matrix is to reduce the phase errors. As seen in the case of 4x4 Butler matrix the phase errors accumulate resulting in too large phase errors across the required bandwidth. Since the smallest

progressive phase shift for an 8x8 Butler matrix is 22.5 degrees, phase errors need to be reduced in the full design.

6.3. 16X16 Butler Matrix

The layout of 16-input, 16-output Butler matrix can get too tedious if same approach is followed as for 4x4 and 8x8 Butler matrices. Moreover the board size would be too large. Another way to design 16x16 Butler matrix is to use a row card configuration as shown schematically in **Figure 6-6**. Each board is a 4x4 Butler matrix. **Figure 6-7** shows how this configuration would look like with the actual design.

Inputs are on the side where each 4x4 board is oriented horizontally and outputs are on the vertical side. The first output port of each of the 4x4 horizontal board is connected to the 4 inputs of the first 4x4 vertical board. Similarly the second output port of each of the horizontal board is connected to the inputs of the second vertical board and so on.

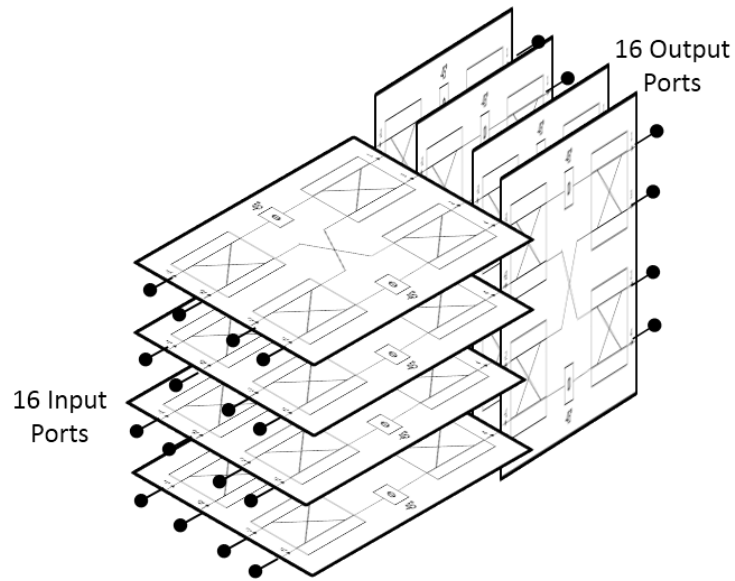


Figure 6-6 : Schematic view of row card configuration of 16x16 Butler matrix from 4x4 Butler matrix

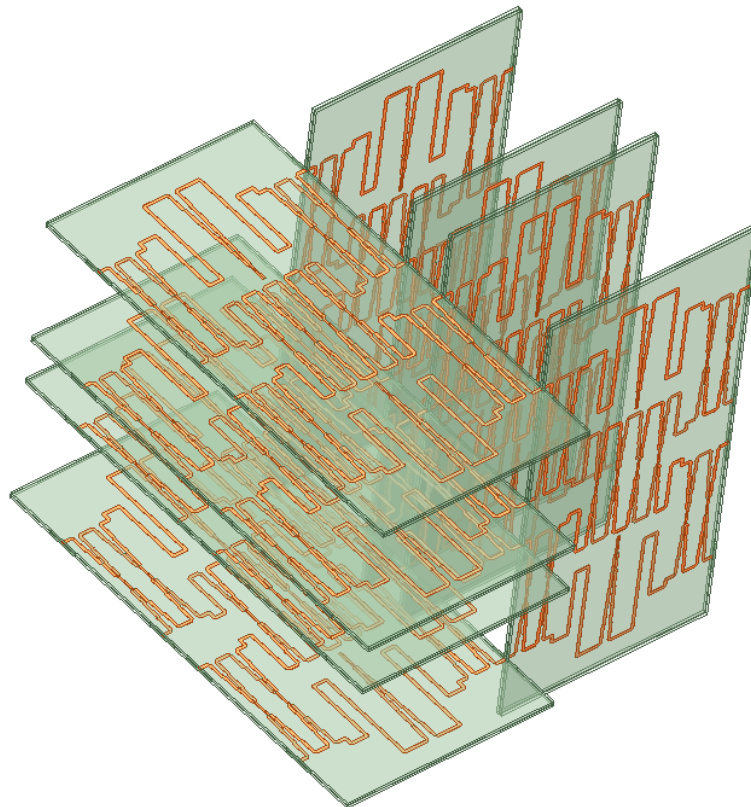


Figure 6-7 : Designed 4x4 Butler matrix stacked in row-card configuration to form 16x16 Butler matrix

An ideal circuit simulation was run for such a design of 16x16 Butler Matrix as shown in **Figure 6-8**. Magnitude response with respect to Port 1 in **Figure 6-9** shows equal distribution of power and the phase response with respect to Port 1 in **Figure 6-10** shows constant progressive phase shift of 11.25 degrees.

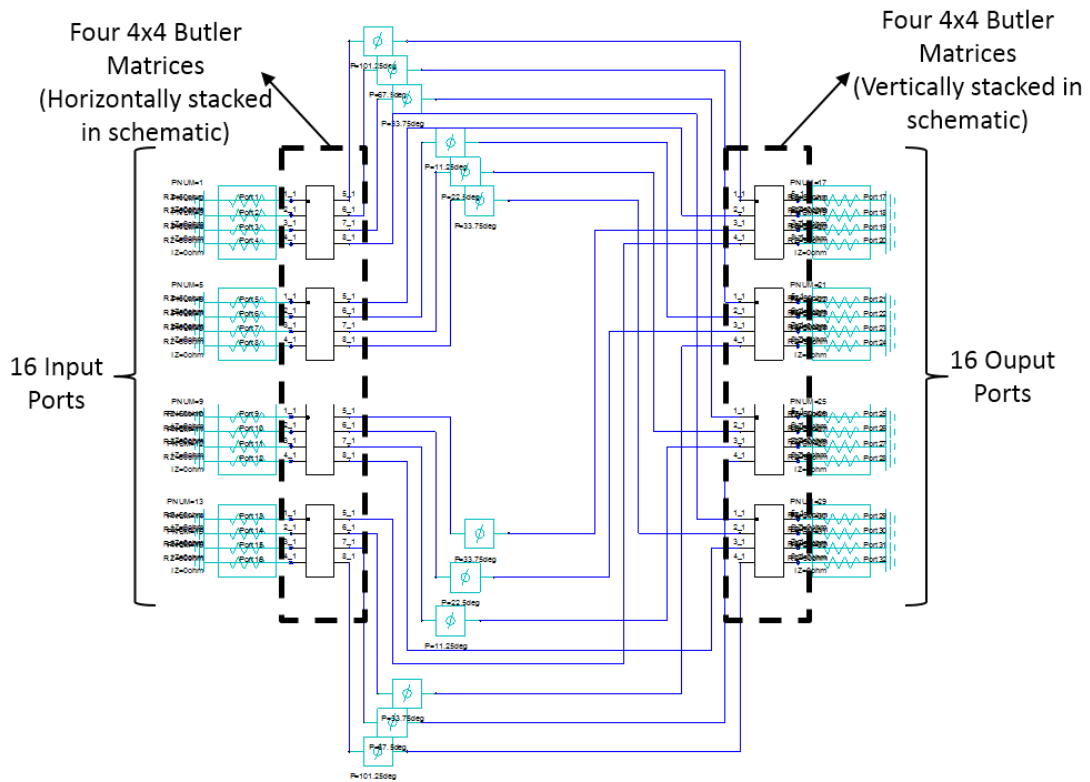


Figure 6-8 : Circuit schematic of 16x16 Butler matrix from 4x4 Butler matrices

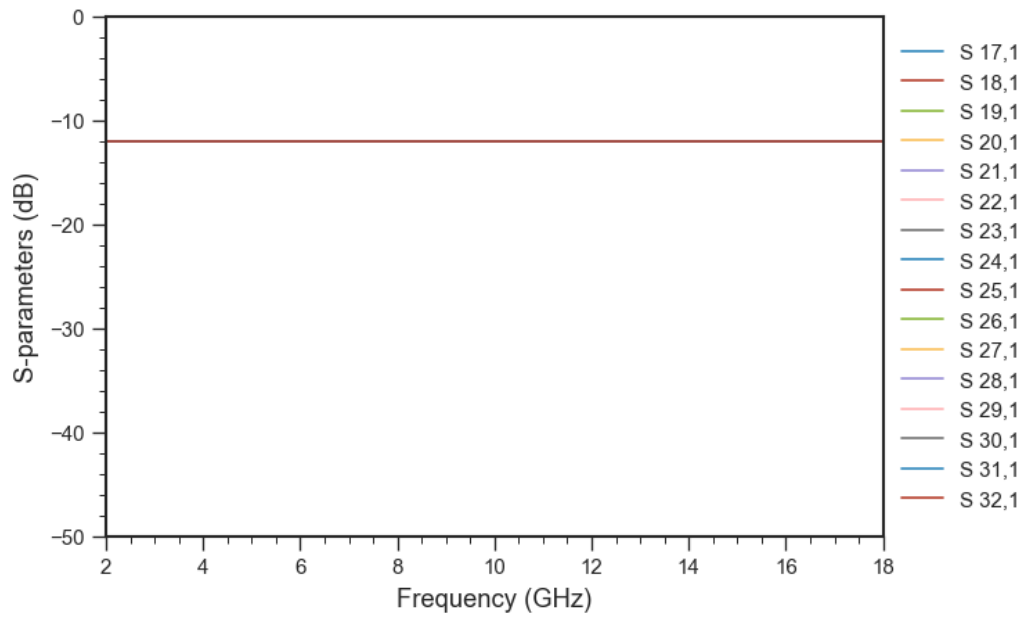


Figure 6-9 : Ideal magnitude response of 16x16 Butler matrix designed as row card configuration of 4x4 Butler matrix

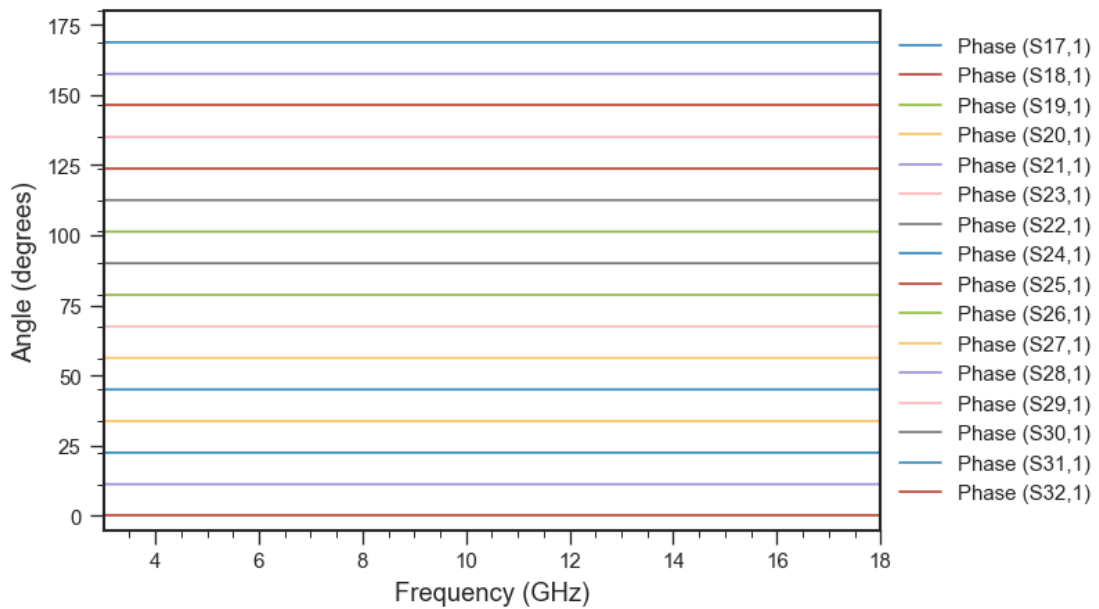


Figure 6-10 : Ideal phase response of 16x16 Butler matrix designed as row card configuration of 4x4 Butler matrix

6.4. 64X64 Butler Matrix

A 64-input, 64-output Butler matrix can be designed following similar design paradigm as in last sub-section. Building blocks for this Butler matrix would be the 8x8 Butler matrix. A schematic construction similar to 16x16 Butler matrix is shown in **Figure 6-11**.

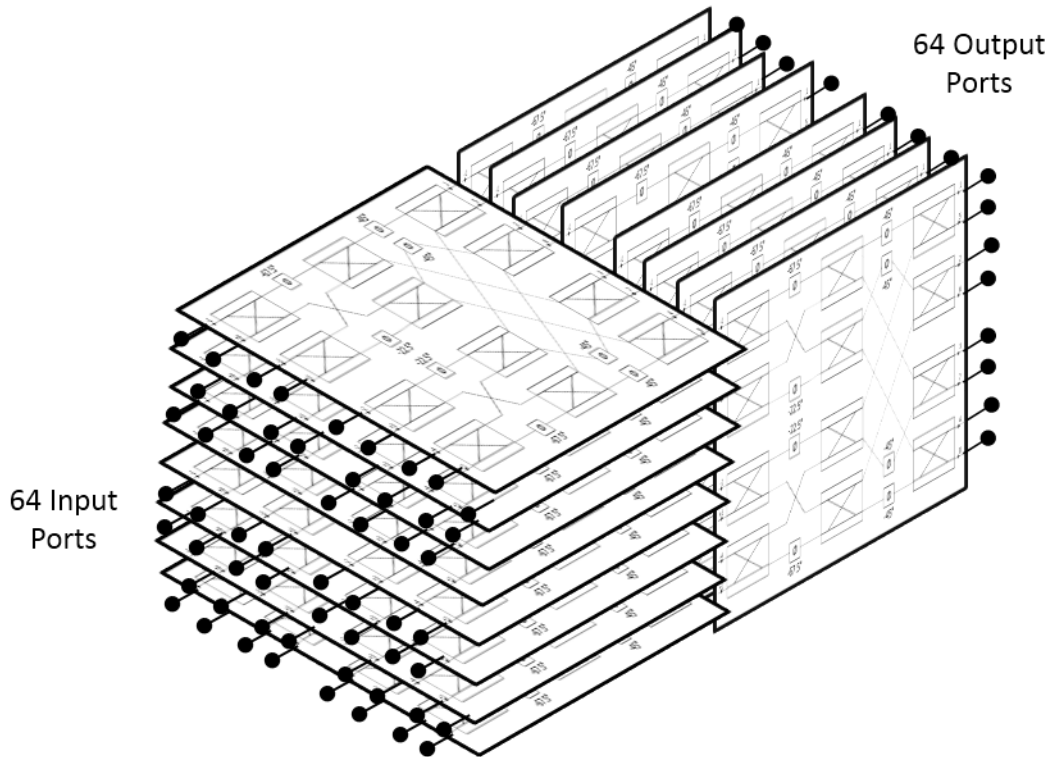


Figure 6-11 : Schematic view of row card configuration of 64x64 Butler matrix from 8x8 Butler matrix

7. CONCLUSIONS

Design of ultra-wideband hybrid coupler, crossover and phase shifters has been presented in this thesis, as a requirement for the design of ultra-wideband Butler matrix. Hybrid coupler achieves tight coupling of 2.6 dB to 3.7 dB across the required bandwidth of 2-18 GHz with a phase error of ± 3 degrees between the coupled and through port. The hybrid coupler is extremely small in terms of physical size (3.1mm x 9.8 mm) as compared to previously designed coupler for such an ultra-wideband range. The phase shifter has been designed as a multi-section Schiffman phase shifter which was shown to have a constant phase shift of 45 degrees across 2-18 GHz with phase error of ± 5 degrees.

Using the designed hybrid coupler, crossover and phase shifter an ultra-wideband 4-input, 4-output (4x4) Butler matrix has been designed and phase response shows progressive phase shifts.

This work also lays down the foundation for the designs of ultra-wideband 8x8, 16x16 and 64x64 Butler matrices.

REFERENCES

1. Bekkerman, I. and J. Tabrikian, *Target Detection and Localization Using MIMO Radars and Sonars* %J *Trans. Sig. Proc.* 2006. **54**(10): p. 3873-3883.
2. Khan, R., et al., *Target detection and tracking with a high frequency ground wave radar.* IEEE Journal of Oceanic Engineering, 1994. **19**(4): p. 540-548.
3. Rahimian, A., *Microwave Beamforming Networks for Intelligent Transportation Systems.* 2012.
4. Rashid-Farrokhi, F., K.J.R. Liu, and L. Tassiulas, *Transmit beamforming and power control for cellular wireless systems.* IEEE Journal on Selected Areas in Communications, 1998. **16**(8): p. 1437-1450.
5. Roh, W., et al., *Millimeter-wave beamforming as an enabling technology for 5G cellular communications: theoretical feasibility and prototype results.* IEEE Communications Magazine, 2014. **52**(2): p. 106-113.
6. Steyskal, H., *Digital beamforming antennas.* Microwave journal, 1987. **30**(1): p. 107-124.
7. Butler, J. *Digital, matrix and intermediate-frequency scanning.* in *1965 Antennas and Propagation Society International Symposium.* 1965. IEEE.
8. Blass, J. *Multidirectional antenna-A new approach to stacked beams.* in *1958 IRE International Convention Record.* 1966. IEEE.
9. Rotman, W. and R. Turner, *Wide-angle microwave lens for line source applications.* IEEE Transactions on antennas and propagation, 1963. **11**(6): p. 623-632.
10. Luneburg, R.K., *Mathematical theory of optics.* 1964: Univ of California Press.
11. Sheleg, B., *A matrix-fed circular array for continuous scanning.* Proceedings of the IEEE, 1968. **56**(11): p. 2016-2027.
12. Denidni, T.A. and T.E. Libar. *Wide band four-port Butler matrix for switched multibeam antenna arrays.* in *14th IEEE Proceedings on Personal, Indoor and Mobile Radio Communications, 2003. PIMRC 2003.* 2003. IEEE.
13. Nedil, M., T.A. Denidni, and L. Talbi, *Novel Butler matrix using CPW multilayer technology.* IEEE Transactions on Microwave Theory and Techniques, 2006. **54**(1): p. 499-507.

14. Butler, J. *Beam-forming matrix simplifies design of electronically scanned antennas*. 1961.
15. Cristal, E.G. and L. Young, *Theory and tables of optimum symmetrical TEM-mode coupled-transmission-line directional couplers*. IEEE transactions on Microwave Theory and Techniques, 1965. **13**(5): p. 544-558.
16. Moscoso-Martir, A., I. Molina-Fernandez, and A. Ortega-Monux, *High performance multi-section corrugated slot-coupled directional couplers*. Progress In Electromagnetics Research, 2013. **134**: p. 437-454.
17. Lange, J., *Interdigitated stripline quadrature hybrid (correspondence)*. IEEE Transactions on Microwave Theory and Techniques, 1969. **17**(12): p. 1150-1151.
18. Abbosh, A.M., M.E.J.I.T.o.M.T. Bialkowski, and Techniques, *Design of compact directional couplers for UWB applications*. 2007. **55**(2): p. 189-194.
19. Abbosh, A., M.J.M. Bialkowski, and O.T. Letters, *Design of ultra wideband 3DB quadrature microstrip/slot coupler*. 2007. **49**(9): p. 2101-2103.
20. Seidel, H.J.I.T.o.M.T. and Techniques, *Synthesis of a class of microwave filters*. 1957. **5**(2): p. 107-114.
21. Jones, E.J.I.T.o.M.T. and Techniques, *Coupled-strip-transmission-line filters and directional couplers*. 1956. **4**(2): p. 75-81.
22. Cohn, S.B., *Characteristic Impedances of Broadside-Coupled Strip Transmission Lines*. IRE Transactions on Microwave Theory and Techniques, 1960. **8**(6): p. 633-637.
23. Hilberg, W., *From approximations to exact relations for characteristic impedances*. IEEE Transactions on Microwave Theory and techniques, 1969. **17**(5): p. 259-265.
24. Shelton, J.P., *Impedances of offset parallel-coupled strip transmission lines*. IEEE Transactions on Microwave Theory and Techniques, 1966. **14**(1): p. 7-15.
25. Anselmi, M., et al. *Design and Realization of 3 dB hybrid stripline coupler in 0.5–18.0 GHz*. in *2014 44th European Microwave Conference*. 2014. IEEE.
26. Schiffman, B.J.I.T.o.M.T. and Techniques, *A new class of broad-band microwave 90-degree phase shifters*. 1958. **6**(2): p. 232-237.
27. Quirarte, J.R., J.P.J.I.t.o.m.t. Starski, and techniques, *Novel Schiffman phase shifters*. 1993. **41**(1): p. 9-14.

28. Schiffman, B.M., *Multisection Microwave Phase-Shift Network (Correspondence)*. IEEE Transactions on Microwave Theory and Techniques, 1966. **14**(4): p. 209-209.